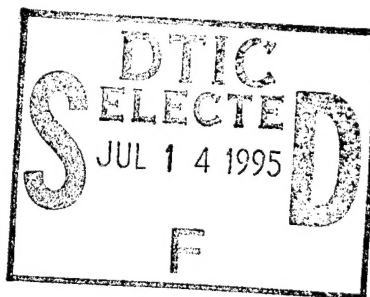Defense Nuclear Agency
Alexandria, VA 22310-3398

DNA-TR-93-155

Particulate Cloud Data Review, Validation, Processing and Planning

John E. Cockayne
Science Applications Intl Corp
P.O. Box 1303
McLean, VA 22102

DTIC
SELECTED
JUL 1 4 1995
F

July 1995

Technical Report

*Original contains color
plates: All DTIC reproduct-
ions will be in black and
white*

CONTRACT No. DNA 001-91-C-0156

19950711 020

DTIC QUALITY INSPECTED 5

DISTRIBUTION LIST UPDATE

This mailer is provided to enable DNA to maintain current distribution lists for reports. (We would appreciate your providing the requested information.)

☐ Add the individual listed to your distribution list.

☐ Delete the cited organization/individual.

☐ Change of address.

NAME: _____

ORGANIZATION: _____

OLD ADDRESS	CURRENT ADDRESS
_____	_____
_____	_____
_____	_____

TELEPHONE NUMBER: (___) _____

| DNA PUBLICATION NUMBER/TITLE | CHANGES/DELETIONS/ADDITIONS, etc.) |
	(Attach Sheet if more Space is Required)
_____	_____
_____	_____
_____	_____

DNA OR OTHER GOVERNMENT CONTRACT NUMBER: _____

CERTIFICATION OF NEED-TO-KNOW BY GOVERNMENT SPONSOR (if other than DNA):

SPONSORING ORGANIZATION: _____

CONTRACTING OFFICER OR REPRESENTATIVE: _____

SIGNATURE: _____

CUT HERE AND RETURN

REPORT DOCUMENTATION PAGE

Public reporting burden for this collection of information is estimated to average 1 hour per response, including the time for reviewing instructions, searching existing data sources, gathering and maintaining the data needed, and completing and reviewing the collection of information. Send comments regarding this burden estimate or any other aspect of this collection of information, including suggestions for reducing this burden, to Washington Headquarters Services, Directorate for Information Operations and Reports, 1215 Jefferson Davis Highway, Suite 1204, Arlington, VA 22202-4302, and to the Office of Management and Budget, Paperwork Reduction Project (0704-0188), Washington, DC 20503.

1. AGENCY USE ONLY *(Leave blank)*	2. REPORT DATE 950701	3. REPORT TYPE AND DATES COVERED Technical 910924-931024

4. TITLE AND SUBTITLE

Particulate Cloud Data Review, Validation, Processing and Planning

5. FUNDING NUMBERS

C -DNA 001-91-C-0156
PE -62715H
PR -RA
TA -RG
WU -DH314260

6. AUTHOR(S)

John E. Cockayne

7. PERFORMING ORGANIZATION NAME(S) AND ADDRESS(ES)

Science Applications Intl Corp
P.O. Box 1303
McLean, VA 22102

8. PERFORMING ORGANIZATION REPORT NUMBER

SAIC - 93/1194

9. SPONSORING/MONITORING AGENCY NAME(S) AND ADDRESS(ES)

Defense Nuclear Agency
6801 Telegraph Road
Alexandria, VA 22310-3398
SPWE/Byers

10. SPONSORING/MONITORING AGENCY REPORT NUMBER

DNA-TR-93-155

11. SUPPLEMENTARY NOTES

This work sponsored by the Defense Nuclear Agency under RDT&E RMC Code B4662D RA RG 00263 4400A AC 25904D.

12a. DISTRIBUTION/AVAILABILITY STATEMENT

Approved for public release; distribution is unlimited.

12b. DISTRIBUTION CODE

13. ABSTRACT *(Maximum 200 words)*

This effort continued assembling the still-available measurements from selected nuclear and large chemical explosion clouds. This empirical data base both helps interpret model predicted effects and validate the predictions. The test were selected after screening many events for data completeness of both the inputs and outputs for the DICE/MAZ and TASS hydrocodes. These are used to calculate the rise and stabilization of the fireball and cloud.

The effort's focus was the particles in the dust dominated and water/ice dominated clouds. This report discusses some archive searches, the limitations of further comparisons of adaptively gridded outputs with measurements, and simultaneous gas and dust measurements in the 10 June 1993 event, MINOR UNCLE. The dust and ANFO by-products were characterized between 0.5 and 2.5 hr after burst by making 10 or more passes at two altitudes in the severely sheared cloud. The repeated passes are used to get good data on radial diffusion behavior in the free troposphere, which can also be used for statistically validating model outputs.

14. SUBJECT TERMS

TASS PRISCILLA	HE Cloud Gases	Atmosphere Nuclear Tests
KING Validation	MINOR UNCLE	Pacific Shots 1 and 2
PROBE DICE-MAZ	Nuclear Clouds	Particle Size Distribution
	Upper Air Data	In situ Sampling by NCAR

15. NUMBER OF PAGES 64

16. PRICE CODE

17. SECURITY CLASSIFICATION OF REPORT	18. SECURITY CLASSIFICATION OF THIS PAGE	19. SECURITY CLASSIFICATION OF ABSTRACT	20. LIMITATION OF ABSTRACT
UNCLASSIFIED	UNCLASSIFIED	UNCLASSIFIED	SAR

CLASSIFIED BY:

N/A since Unclassified.

DECLASSIFY ON:
N/A since Unclassified.

PREFACE

Accesion For		
NTIS CRA&I	☑	
DTIC TAB	☐	
Unannounced	☐	
Justification		
By		
Distribution /		
Availability Codes		
Dist	Avail and / or Special	
A-1		

CONVERSION TABLE

Conversion Factors for U.S. Customary to metric (SI) units of measurement:

Multiply TO GET $\longrightarrow$ $\longleftarrow$	By By $\longrightarrow$ $\longleftarrow$	TO GET Divide
British thermal units (Btu)	$1.054\,350 \times E+3$	kiloJoule (kJ)
calorie (thermochemical)	$4.184\,000$	joule (J)
calorie/second (cal/sec)	$4.184\,000$	Watt (W)
atmosphere (normal)	$1.013\,250 \times E+2$	kiloPascal (kPa)
foot (ft)	$3.04\,8\,000 \times E-1$	meter
foot^2 (ft^2)	$9.290\,304 \times E-2$	meter^2
foot^3 (ft^3)	$2.831\,685 \times E-2$	meter^3
pound-mass (lbm)	$4.535\,924 \times E-1$	kilogram (kg)
pound mass/foot^3 (lbm/ft^3)	$1.601\,846 \times E+1$	kilogram/meter^3(kg/m^3)
cubic feet/minute (cfm)	1.6992	meter^3/hr
gallon/minute (gpm)	0.2271	meter^3/hr
centipoise (cp)	0.001	kg/m-sec
mile/hr (mph)	0.447	meter/sec (m/s)
nautical mile/hr (knot)	$18.52/36$	meter/sec (m/s)
pound/square-inch (psi)	6.895	kiloPascal (kPa)
inches of water (inches-H$_2$O)	0.2491	kiloPascal (kPa)
inches of mercury (inches-Hg)	3.3870	kiloPascal (kPa)
British thermal units (Btu)	$1.054 \times E+3$	kiloJoule (kJ)
horsepower (hp)	$0.746 \times E-3$	Watt (W)
degree Fahrenheit (°F)	$T_K = (T°F + 459.67)/1.8$	[degree] Kelvin (K)
Btu/lbm	2.326	kJ/kg
Btu/hr-ft-°F	1.731	W/m-°C
Btu/lbm-°F	4.187	kJ/kg-°C
Btu/hr-ft^2	3.15	W/m^2
Btu/hr-ft^2-°F	5.67	W/m^2-°C
cal/cm^2-sec	$4.184 \times E+4$	W/m^2
cal/cm^2	$4.184 \times E+4$	W-sec/m^2

TABLE OF CONTENTS

TABLE OF CONTENTS (Continued)

FIGURES

SECTION 1

INTRODUCTION

1.1 PROGRAM GOAL.

For more than 20 years, the Defense Nuclear Agency has steadily issued contracts to develop hydrodynamic models, the so-called hydrocodes. The pertinent ones predict the evolution of the particulate cloud, especially dust and precipitation, from the stage of a burnout sphere following a surface interacting nuclear burst until after the cloud's vertical and horizontal stabilizations.

> ...(such)..."models were state of the art and our computers never dropped a
> digit. Of course, ...our models were no better than the assumptions that went
> into them--a model, after all, is nothing but a best-guess simulation of a world
> you've never seen, based on experience with a world you don't really
> understand all that well. And since, in many cases, any of several guesses are
> equally plausible, why not pick the ones that best help produce the answer that
> the big guns...are shooting for?" (Allen, 1993).

This pessimism might apply to these fireball/cloud hydrocodes because of the strong sensitivities of the output to the model parameterizations and to the many pertinent inputs. Reasonable approximations or parameterizations have had to be developed for the many probable and potential processes addressed, even when explicit calculation of the radiation transport has been excluded. The repetitive iteration of the hydrocode development with a reality check continues currently by critically comparing the code outputs with the limited measurements of cloud properties.

This current contract's two year evaluation of the MAZ and TASS development efforts emphasized a more detailed early time bomb debris comparison for the King airburst of Operation IVY, the detailed dust particle size distribution (PSD) comparison for the MINOR SCALE burst of ANFO high explosive (HE), and an in-progress detailed ice crystal PSD comparison for the Pacific Shot #2 (PS2) event. In addition, this particulate cloud review effort emphasized late time cloud validation data availability by reducing both multi-gas and small dust dispersion/diffusion data obtained from about 0.5 to 2.5 hr after an ANFO HE burst in 1993 called MINOR UNCLE. Miscellaneous minor items were also addressed under the two tasks entitled "Data Review" and "Validation Cases," which attempted to maintain coordinated understanding among the multiple authors of DNA supported publications and databases regarding dust, etc. particulate clouds.

Given the very skewed and small set of real terrains (i.e., soils and any coverings) and actual upper air profiles for the atmospheric nuclear explosions done about 30-50 years ago by the United

1

States, and given the dust cloud hydrocode complexity, more confidence is required in the fireball/cloud hydrocodes before they can be automatically applied to current particulate problems of national importance without a major peer review. Obviously it has been decades since the last pertinent United States atmospheric nuclear tests with a significant amount of cloud geometry or more particulate oriented observations. Due to the absence at that time of any interest in the particles per se, an integrated effort is now needed to achieve the retrieval and authentication of all available and relevant measurements for hydrocode validations.

The documented data that are retrieved from the archives should pertain primarily to the prediction of the particulate concentrations/size distributions/locations and the flow field that lifts the particles to high altitudes before both the mean and mixing flows are stabilized. Other observations of output trends and of reality are also useful in searching for any inconsistencies as the post facto method for achieving validation of the hydrocodes by empirical data.

The current particulate cloud review and associated validation effort is concerned both with the MAZ shock hydrocode, which is a major revision in some parts of the DICE shock hydrocode, and with the SAIC-developed version of the TASS meteorological hydrocode, which is an expanded version of the TASS used by NASA and FAA for non-nuclear convective clouds and also for large downbursts. Some other pertinent shock hydrocodes developed for the pertinent significant particulate interactions are the SHELL, HULL and SHARC family.

1.2 BACKGROUND.

Using a large input set of initial and boundary conditions, the hydrocodes (for moving uncharged particles) solve simultaneously both the coupled set of mass, momentum and energy conservation equations **plus** postulated parameterizations for many complex processes. Some such complex phenomena are two soil separations, into more volatile species and into sub-clumps of the continuum ejecta, and two soil phase changes from mixed mineral melting through element vaporization and condensation. For the nuclear explosion cloud application, the four (/five for 3-D) differential conservation equations generate large instantaneous rates in the transition to a perfect late time sink-and-source exchange rate so that all of the change-forcing differentials are essentially zero, or at least less than the dynamics inherent in the background flow of the atmosphere.

The changing dominance of the different destruction and production rate terms in the differential equations implies that most of the specific properties change by over a factor of 100. Given the continuing evolution or incompleteness of the submodels and the inherent limitations of computer approaches, there will always be an open question regarding convergence on the physical reality by the hydrocode output. The nuclear cloud community is in the position that a good understanding of the physical reality is difficult due the very limited observations of pertinent particles.

2

The verification and so-called validation of all large computer codes has intensified even more in the last decade as computational fluid dynamics has evolved as a field of discipline. The evaluation of model fields (i.e., grided outputs of hydrocodes) is now an important discipline in meteorology (Oreskes et al., 1994), of which the nuclear fireball/cloud problem is a specialized extension due to the source's initial power per unit volume. Murphy (Murphy, 1991) has spent years systematically defining the scientific basis for this evaluation because the weather 'system' is open--all sinks and sources are not known. The almost ad hoc status of most previous evaluations will presumably soon become standardized. This standardization is the potential route to a broad community confidence in the self-imposed verification and validation efforts by the hydrocode developers.

The key items in the Murphy method for evaluating model outputs are the formalized groupings of the comparison's complexity and dimensionality. Complexity depends on the number of factors affecting the time independent information involved in an absolute evaluation of output against reality. That is, a joint distribution $p(f,m)$ of the predictions or forecasts (f), and of observations or measurements (m), can be factored into its respective conditional [i.e., $p(x$ given $y) = p(x|y)$] and marginal [i.e.,$p(y)$] distributions, either as '$p(m|f)p(f)$' or as '$p(f|m)p(m)$.' More methodology details were previously presented to the dust cloud community (Cockayne, 1993). At that time, it was thought to be too expensive to perform such an evaluation at this stage of the modeling that consists of a more exploratory development than of a confirmatory comparison of the calculations.

Given the generally chaotic mixing or turbulent nature of the fireball/cloud flow field, Murphy's totally statistical perspective is needed despite the deterministic inputs. The usual approximation of the flow by an axi-symmetric geometry also encourages a stochastic scheme in order to finesse the issue of accurate averaging for the third dimension in the real world. The result is that the model or code evaluation and confidence building is an extensive effort when done systematically using many detailed observables. A major limitation of this approach occurs when only a few pertinent observables are available, such as for those nuclear clouds with significant particulate mass. With further development by Murphy, the technique could presumably handle such sparse data cases.

An approach developed by Flueck (Flueck, 1989) with more adaptability is presented in the following **Table 1-1** for the classification of comparison techniques by the degree of objectivity and by the class of study (i.e., confirm a model, or only obtain data for modeling guidance). Such a classification procedure removes the vagueness of the achievement from each comparison. The key feature of this table is the clear discrimination of whether an investigation goal is more oriented to searching for (or parameterizing) missing processes, or oriented to certifying the accuracy of the modeling. The PROBE code (Hillendahl, 1994) permits the first objective MAZ field comparison.

The first phase in evaluating any hydrocode's convergence on physical reality is the **verification** of the output for some simple specific pseudo-physical problem (PPP) being modeled by the

Table 1-1. Classification of comparison techniques.

	Exploratory	**Confirmatory**
Subjective	1. Visual, seems "realistic"	1. Visual comparison of a sequence of paired fields
	2. Visual comparisons of a forecast to the observations	2. Visual comparisons for a randomly selected set of paired fields
Objective	1. Mean square error, mean error, correlation	1. Stratified random sampling estimation
	2. Anomaly measures of field	2. Split sample comparison

hydrocode. The classical approach for verification is solving a suite of PPPs that have either analytical solutions or alternate numerical simulations that are both accurate and precise within the available computer precision. The next significant level of confidence via verification above the simple PPPs is solving a suite of defined semi-real problems and comparing the outputs with alternate hydrocodes that use the same inputs and parameterizations, but usually with different implementations. This confidence level step is generally given lower priority for funding by the DNA sponsor than the next step of a first empirical level validation by observations.

The second phase in evaluating the code convergence on reality is a so-called **validation** with measurements. The difficulty starts with the question of what item is pertinent to validate in the hydrocode, or, more importantly, what can be validated by observations in the case of nuclear clouds. The central issue is that the numerical model is neither as complete nor detailed as possible for the current state of knowledge. Thus, by definition, the approximations and very reasonable parameterizations can easily be found to fail a case type validation. This is actually an advantage.

The real advantage of case validations is that any lack of success implies an explicit opportunity to make a minor or even major modeling improvement. The change can be just a so-called tuning-up, the negativism of which can be offset totally by rerunning EVERY previous validation using the improved model and still obtaining as good validations as originally obtained. The risk is that the rerunning can uncover incompatibilities in the parameterizations that require serious redevelopment efforts. Nevertheless, this iteration with reality from an expanding empirical basis eventually will become an asymptotic approach to the model's refinement. Unless the rerunning is very thorough, the many modeling improvements will likely diverge into an incompatible set of program patches. An alternative leads to emphasis on comparisons with ensembles of data from many experiments. As it turns out, such an ensemble level is also usually cost effective for the pertinent systems level

4

calculations by a nuclear cloud hydrocode because other problem input variations control the output uncertainty. The result is that the degree of evaluation or validation varies widely and usually in some proportion to the potential bad results from either bias or incorrect sensitivity to some factors.

1.3 SPECIFIC OBJECTIVES.

Due to the existence of an all weather booster/reentry body/vehicle, more cloud accuracy and precision are needed for soil and water/ice particles. Two topics that are interactively involved in predicting the missile damaging clouds are the particulate-laden flow field and the life cycles of the real dust/water/ice particles. The latter topic produces both significant soil effects on the fireball flow and early relative buoyancy field as well as significant water/ice effects on the later cloud rise and stabilization flow field. The net result is that a multi-step validation program for a fireball/cloud hydrocode needs to initially avoid large flow field impacts from any uncertain particle processes. Structuring a systematic scheme for achieving validation of the pertinent hydrocodes is the starting point for the general program that involves the particulate cloud reviews.

The specific objectives of the tasks in this particulate cloud review contract were to:
- "review available experimental data which is relevant to nuclear particulate (e.g., dust, pebbles, water, and ice) cloud formation and dissipation. ... include nuclear data, high explosive data, and laboratory data. ...evaluate the consistency of the data and identify shortcomings in the knowledge base."
- "define several experimental cases for use in validating particulate environment predictions. ...selected to include as much of the relevant physics as possible. ...identify the pertinent experimental data set and will provide the information required to initialize the corresponding environment prediction...."
- "recommend and prioritize future cloud environment experiments with the intent of reducing the shortcomings identified...and developing validation cases similar to Task 2. ...conduct preliminary test planning for the most promising experiments...."

The second task included a major effort to reduce recent measurements of HE fireball gases and dust, etc. particles that were translating and diffusing in the lower free troposphere (i.e., starting above the planetary boundary layer). That effort is reported in detail within the Proceedings of the MINOR UNCLE Symposium in early 1994 (Cockayne and Edwards, 1994).

This report is arranged as follows: section 2 discusses the various data forms used for particulate cloud reviews, section 3 summarizes the miscellaneous activities for the data review task, section 4 summarizes the miscellaneous activities for the validation task, section 5 reviews the work done on the MINOR UNCLE Dust Cloud Atmospheric Transport (MUDCAT) project, section 6 provides a summary and conclusions, section 7 provides recommendations, and section 8 lists the references.

SECTION 2

PROCEDURE

2.1 OVERVIEW.

2.1.1 Introduction.

The coupling into the gaseous flow field dynamics (**FFD**) of the particle production, momentum of high kappa regions (dust density $\geq$ gas density), and dust-absorbed thermal radiation adds complications to the already transient evolution of the turbulence. The FFD decoupling from any significant dust particle involvement can be achieved by using a high scaled height of burst. An intermediate involvement of dust in the FFD can be partitioned into air bursts with and without a major fireball interaction with the ground, such as a partitioning around the fallout free burst height of about 55 m/kT$^{0.4}$. An intensive involvement of dust and ejecta in the FFD can be partitioned into ejecta producing bursts with and without a major portion of the x-ray and neutron energy initially deposited in the ground. Shallow buried bursts that still produce high altitude dust clouds are the 'near-surface' bursts with major initial bomb energy depositions directly in the soil with a resulting jump in the ejecta volume for essentially the same size fireball.

The total decoupling from any major water/ice particle involvement in the FFD either requires relatively low cloud stabilization heights or a relatively dry ambient air mass around and above the burst. A significant involvement of the water/ice in the FFD occurs when the air mass is relatively moist around and just above the height of burst. A special case of significant water/ice particle involvement occurs when natural clouds are entrained into the rising fireball/nuclear cloud. The net result of categorizations is the following **Table 2-1** of 20 pertinent combinations, of scaled height of burst (SHOB) and of stability/conditional stability, for the validations of the FFD through the cloud stabilization time; the increasing numbers roughly represent increasing complexity of the nuclear cloud physics.

The start of this multi-contractor validation effort in 1989, under a previous two year contract, was when the focus of the hydrocode production cases for fratricide studies was mostly on the lower central matrix cells 10-11 and 14-15. The former category is focussed on the hydrodynamically scaled heights of burst of 50 and 120 ft/kT$^{1/3}$ (i.e., ~15 and ~37 m/kT$^{1/3}$). Both SHOBs have a significant reverse vortex, with distinctly different character and strength, that is produced from the spherically radial flow in the downward moving blast wave encountering its own significant reflection by the ground or water. This strong supplementary but transient vortex adjacent to the ground or water is the primary initial particle lofting and mixing mechanism after the soil is scoured by the blast wave or otherwise lofted into the bottom layer of air.

6

Table 2-1. Case numbering for discussing the validations of MAZ and TASS.

<u>**Water and Ice Effect Categories**</u>

Dust Effect Cat.'s	**Small Rise Height**	**Relatively Dry Amb. Air**	**Relatively Moist Amb. Air**	**Cloudy & Moist Amb. Air**
Free-air Burst	1	2	3	4
Fallout-free Burst	5	6	7	8
Reverse-vortex Burst	9	10	11	12
Surface Burst	13	14	15	16
Shallow-buried Burst	17	18	19	20

All the cells 13-16 for surface bursts imply two regions that are cooled significantly by the ejecta injection: one is confined around the primary elevation angle (i.e., 45° for saturated soils) and the second is under that cooled conical region when the slower/slowed down ejecta achieves apogee and falls out of the fireball during its initial rise. The initial fireball rise is significantly delayed in spite of the extreme buoyancy due to the virtual mass effect and the relatively long time it takes for ambient air to laterally force itself completely under the ~1 km radius fireball using the weak force of buoyancy after the blastwave motions decrease. Also note that the ejecta injection sets up strong vortices within the fireball both above and below the initial conical shell or layer of soil. These two vortical flows must be reversed and reorganized, respectively, in the transition to the dominating toroidal vortex when the initial fireball rise finally accelerates and starts entraining ambient air.

The net result is that the air burst and surface burst flow fields are very transient even without the locally large latent heat effects from the evaporating and recondensing soil constituents. With this understanding, the validation was approached in two phases: first, address the FFD validation without the complications of large soil loadings, with and without water/ice particulate production impacts, and then progress to the high soil loading case validation.

The issue of verification and validation again arises after the above overview of the state of the knowledge. In section 1.2, verification was addressed in the context of any numerical solution being the true result for the full equation set in the model. "In contrast to the term verification, the term validation does not necessarily denote an establishment of truth.... Rather, it denotes the establishment of legitimacy,... a model that does not contain known or detectable flaws and is internally consistent can be said to be valid." (Oreskes et al., 1994) However, validation must interact with the separate physical verification issue that concerns correspondence of the complete equation set to the true material reality at all times/places. This perspective provides an outline for progressing from the simple to the complex cases. Likewise, it highlights the importance of using a

wide variety of cases even within each cell of Table 2-1 in order to thoroughly test for the detectable flaws and internal consistency. This forms the outline for the next three sections.

2.1.2 Free-Air and Fallout-Free Bursts.

The clean or dust-free fireball FFD condition occurs for all of the cases in the top two rows of the above Table 2-1, which is 40 % of the matrix cells. The Operation UPSHOT-KNOTHOLE Climax airdrop in cell 1 of the above Table 2-1 was addressed previously by Cockayne (Cockayne, 1993) and Hassig (Hassig et al., 1992). The next row of cells 5-8 in the above Table 2-1 has a stronger reflected shock effect but without a significant reverse vortex effect at the ground. In the past, the gun-launched Operation UPSHOT-KNOTHOLE Grable burst of 15 kT was investigated by the hydrocodes due to its dramatically photographed precursor, which had just been recognized in the testing during the previous year due to its increased SHOB to suppress the local fallout.

This second row includes the lowest SHOBs for the balloon supported bursts and the lowest SHOB airdrop. That is, the Operation IVY/King burst was a large pure fission device dropped in November 1952, partially to demonstrate an operational strategic capability. Dropped near the north end of the Runit Island in the Enewetak[1] Atoll, this approximately 500 kT burst had a long time for all absolute and relative buoyancy effects before any swept-up water entered the fireball. This event in cell 6 of the Table 2-1 was also addressed by Cockayne (Cockayne, 1993), Hassig (Hassig et al., 1992) and Bacon (Bacon et al., 1992). What is new is that the best MAZ/updated-DICE code solution was processed by the PROBE code (Hillendahl, 1992) for the first detailed comparison of the early fireball with quantitative field measurements (Hillendahl, 1994). Given a rudimentary radiation loss algorithm in the MAZ code, the large internal temperature discrepancies around 2 sec after burst are apparently explained and potentially resolvable (Hillendahl, 1994).

The inherent variability of cloud behavior for bursts at the same SHOB within row two is a major concern to the validation effort due to the inherently turbulent FFD and the transient FFD nature that has the option for a significant chaos effect (i.e., a later large effect from a small change(s) in inputs). After searching the inventories of all atmospheric nuclear tests for which cloud-related data sets are available, we recommended that three tests over water near an atoll be used for validation in this row of the Table 2-1 in case any one of them turns out to be an exception from the normal capability of the hydrocodes. In addition, the Operation PLUMBBOB Priscilla burst under a balloon over the playa soil of the Frenchman's Flat was set up in 1992 for a verification and validation run by the newly evolving early fireball rise hydrocodes at the Lawrence Livermore National Laboratory. Due to the lack of a scientific film (i.e., dimensions are obtainable) beyond ~70 sec after burst for the Priscilla event, the TASS code could not be well validated despite our obtaining the complete sounding in raw data form from the 'Weather Bureau' archives.[2]

---

[1] Formerly spelled Eniwetok.

[2] Cpt. Vince Jodoin, USAF, kindly copied two microfilm plots at the Air Force Institute of Technology.

8

2.1.3 Reverse-Vortex Bursts.

The row 3 is where the downward blast wave essentially sets up the flow equivalent of a radially expanding jet impinging on a flat plate. This SHOB category generates a transient reverse vortex in the bottom of the fireball that focuses the initial dust lofting or injection into the fireball interior at a ground range of about half of the fireball radius. The initial injected dust concentration is small enough that only some dust is vaporized and the gas temperature still stays up over 1,500 K. The net result is that once the blast wave motions decay, there are strong relative buoyancy effects even within the dusty fireball. These incipient turbulence eddies or turbules are important in setting up the mixing of soil particles with any still clean fireball air and then produce SiO vapor (from the liquid or solid SiO_2) that radiates away energy much better than does air at about 2,500 K. However, this aspect may be less significant than previously perceived if the current MAZ fireball is being kept too hot by a radiation loss algorithm that is too simplified. Subsequently entrained dust can avoid condensing radioactivity due to this quenching effect (Engquist et al., 1951).

The reverse vortex row contains only tower bursts, even for foreign ally nuclear bursts. Many have such large shielding and/or cab masses on the top of the tower that the thermal radiance versus time was significantly modified.[3] In only a few events is the pertinent (cab/shield) mass to yield ratio low enough that the hydrocode can totally ignore the effect of an altered fireball cooling and altered radial temperature profile. Nevertheless, the tower structure and evaporated cab mass interacts with the blast-wave-driven reverse vortex; the shock is attenuated by the reflections from all of the unvaporized truss members (a reflection of a surface reflected shock can loft molten metal), and the promptly vaporized shield/steel near the device has an essentially radial momentum that later affects the flow field out well away from the tower bottom. The result is that the initial buoyancy field and residual blast wave flow field can be unique and complex for every tower test.

The uniqueness of the tower tests leads to the need for special sensitivity runs in order to assess the impact of these effects on the observables. While the tower heights increased from the 100 ft used at TRINITY to 200, 300, 400, 500 and finally one 700 ft tower used at Operation PLUMBBOB Smoky, it was learned that the tower's vaporized/removed portion was generally limited to that within the inner approximately 30 percent of the horizontal fireball radius. Beyond the ~30 percent, the surviving steel structure enhances the turbulence in the stem. This low percentage leads to only one tower effect (i.e., metallic vapor condensation at high temperature) on the FFD for the lowest SHOB cases, such as the TRINITY test, the Operation GREENHOUSE/George event, and the Operation REDWING/Mohawk event; the other tower bursts also have the tower turbulence effect. Thus, yield scaling up to the strategic yields raises resistance to using the other tests of order 10 kT around SHOB = 50 ft/$kt^{1/3}$ for primary validations. Exactly because of that caveat, they are even better candidates for flaw searching in the modeling, even after accounting for the tower effects.

---

[3] "RECIPE Tower Burst Model" briefing to Dr. George Ullrich in 1985; recently funded for publication.

In summary, the MAZ model is not yet capable of modeling the actual processes involved in the nuclear and large HE tests that are in this row of Table 2-1. Once the metallic vapor and tower turbulence processes are added into MAZ, sensitivity studies can be performed to verify that some relatively large yield event has so little impact from both processes that it can be used for a pertinent validation. For example, the Operation GREENHOUSE/George shot of 225 kT on a 200 ft (61 m) tower and Operation REDWING/Mohawk shot of 360 kT on a 300 ft (91 m) tower are candidates, if the cab masses are relatively low, because the stem diameters are relatively large compared to the tower width. Unfortunately, the pertinent Ruby Island in the Enewetak Atoll is so small that most of the sweep-up is water, not soil, which introduces a very different vaporization temperature and associated time/place for the effect of the phase change effect on the pressure and on the thermal energy sink/source. The George cloud was well sampled with good results (Engquist et al., 1951).

2.1.4 Surface and Shallow-Buried Bursts.

The surface burst row is also populated with complex cases when viewed in the context of good validations for calculations of nuclear weapon initiated clouds. That is, some shots used device emplacements and soils that are specialized and any validations using them still has the issue of transferring the model back to the more nominal targeting situations. For example, the JOHNIE BOY event was a sub-kiloton weapon shallow buried in the glass-laden residue of volcanic ash. One result was that the manned in situ sampling of the cloud occurred early enough that the over 100 μm diameter granular particles were still at the aircraft altitude for one pass. On the other hand, the fast early ejecta with small sizes did not stagnate until outside of the fireball. Thus, the initial particle size distribution (PSD) is both unknown and likely to be unique to that event. The six weeks from the start of this shot's planning until detonation led to a modest fallout collection effort, but it was primarily just a practice collection for the SMALL BOY event, which was on a short wooden tower over the playa in the lakebed of the Frenchman Flat at the Nevada Test Site (NTS). The result is that the initial PSD for JOHNIE BOY is hard to infer from the combined air and ground sampling even when a hydrocode is assumed to be correct.

The SMALL BOY event is complicated due to the hydrodynamic effects of its short triangular wooden tower in producing some ejecta of the playa soil. Likewise the BUSTER-JANGLE Sugar event was a 1.2 kT burst in a relatively massive large diameter casing that was setting almost on the ground. Consequently, the hydrodynamics-dominated cratering caused a large mass of low angle, intermediate temperature soil to be injected into a low mass of fireball gas with the probable result that little ejecta experienced ablation or vaporization of the particle surface. The importance of this atypical ablation process is that the current (DICE) MAZ modeling makes all of the small size ejecta particles from condensation of the soil vapors from the larger particles. The uncertainty at Sugar is amplified due to the bulldozed crater and 'shovelled' soil backfill under surface ground zero for a minimally documented LASL experiment. (Personal communication, John Lewis, 1993)

10

The non-NTS surface bursts were mainly on coral and barge/water surfaces; a small event at the PPG was on soil imported from NTS. The on-coral events even included two devices inside of water shielding tanks that enhanced coupling and the ejecta production. The REDWING/Lacrosse event even had a high/large soil mound immediately beside the device for shielding some scientific instrumentation with the result that the fireball/cloud was split initially into two sections. One so-called surface burst validation candidate was set on a concrete post in a concrete pit so the cratering is very unique. In summary, this row has no good candidates for simulating operational cases of interest. Again, exactly because of these caveats, they are even better candidates for flaw searching, which would require a rather large labor effort to do the best calculations for each event.

The fallback cases for the surface burst row are the chemical explosions since ~1970. Also, these shots were frequently on soils that are more interesting than the coral, playa and old volcanic ash mentioned above. The MINOR SCALE (MS) event in 1985 at the White Sand Missile Range was well characterized with two sampling aircraft and thus by default became the best candidate for a surface burst validation. This event was nearly repeated in 1987 by the MISTY PICTURE event except for the fact that there was an ambient water cloud above the burst; thus that portion is a cell 20 case. The lower stem region is mostly a second version of the MS stem, but without the initial inhomogeneities in the MS fireball from the leaked explosives. Finally, the MINOR UNCLE event in 1993 had the same crater size and was sampled until beyond 2.5 hrs after the burst.

In summary, the cells and events for an initial validation effort are as follows:

Cell No.	Event
1	Operation (Op'n) UPSHOT-KNOTHOLE/Climax
6	Op'n IVY/King, Op'n PLUMBBOB/Priscilla & Pacific Shot #2
7	Pacific Shot #1
18	MINOR SCALE and MINOR UNCLE
18	MISTY PICTURE stem (cell 20 for the upper cloud itself)
18	MINOR UNCLE late time cloud top and cloud bottom

2.2 PHOTOGRAPHY.

The fireball/cloud dimensions and shape are the most obvious measures of the small particulate environment. Nevertheless, the edge definition is also one of the hardest items to calculate from the hydrocode outputs of PSDs in cells for both dirt and water-based particles. The latter complicate the validation by modifying the photon beam geometry that irradiates cloud-edge particles and produces the local inherent contrast. This inherent contrast is attenuated for any remotely located film camera or other imagery system, whether surface, aircraft or satellite based. As an interim measure, a basic blockage approach was developed for the pure blue sky that integrates along the many parallel lines of sight through the hydrocode output. By fiat, the edge is located where there

11

is only 10 percent transmission. This OBSCURE post processor code is applied to the one minute and older clouds. There is still also the approach of plotting the 10^{-8} and 10^{-10} g/cc contours for trying to bound the edge. For pre-one minute times, this gradient idea is satisfactory for the upper cloud because the 10^{-8} - 10^{-10} contour spacing is usually near the grid resolution of the hydrocode. For the stem, the apparent absence of any translucent annulus suggests that most of the contours are all within one grid cell, which the model cannot simulate due to the numerical diffusion effects.

The best contrast photography is generally from the still and framing cameras, versus the simpler movie or cine cameras that indicate the flow dynamics. A popular framing camera during the atmospheric nuclear testing was the converted large format reconnaissance camera. To get the best coverage, it was run in its so-called runaway mode to take frames as fast as it could register each frame and take up the exposed frames. The result was that the frames are not timed and the frame intervals are all different. By using the few frames published with times from some still cameras, the sunlight shadow features could be used to assign times for the frames in the runaway film.

The IVY/King coverage also included essentially redundant cameras for early time due to the importance of the thermal radiance history characterization on that large air burst. During our previous contract, we identified two films with 1952 color emulsions that have not been analyzed for the spectra of the fireball and bomb debris when the bomb debris is first photographable. These films taken through different neutral density filters (ND-1, ND-2) retain good contrast/color for this bright source when the debris is first imaged at about 1.35 sec after burst. The visible fireball color and debris images were so unexpected that they were considered a critical validation 'point' for the temperature field in the MAZ hydrocode. Dr. R. Hillendahl of SAIC converted the thermal radiation algorithms in the RECIPE code into a new PROBE code that can produce the color of any picture element on the negative film (Hillendahl, 1992) using the MAZ output for the appropriate time. A quantitative comparison was feasible due to the IVY/King weapon being a 10,000 pound aluminum cased bomb; all of the line and continuum radiation characteristics are known for the aluminum vapor and its high temperature oxides and elemental ions. The result was that the MAZ temperature and air density output file for the best IVY/King run was post processed by the PROBE code, using the RECIPE determined debris and aluminum concentrations, in order to calculate the local transmission and spectrum at 1.82 sec after burst (Hillendahl, 1994).

The feature-matching analysis of a runaway film for the IVY/King event was done where the cloud rise views were obtained from the three close-in aircraft and one ground station. Unfortunately, the planned long range cloud photography aircraft with a good perspective aborted so no view is available with a small elevation angle that permits seeing what the cloud top surface looked like during the later cloud rise and stabilization.

The primary CLIMAX photography around dawn is the self luminous black and white film, which (along with another film) was previously analyzed for radiance contours. Due to the currently

inadequate MAZ parameterization for the flux history, any radiance comparison should wait until MAZ is changed and rerun for CLIMAX. Then, once the PROBE code is upgraded to handle the rays converging on a camera, the radiance contours can be compared in extensive spatial and temporal detail to the post processed output of MAZ.

The other KING-like airbursts are limited to one surface station for the photography of the mid-ocean atmospheric nuclear tests. In one case, there is also an airborne camera at long range. This is especially helpful due to the low elevation angle to the cloud top, with the result that any axial bulge or overshooting could be seen and compared to the code output.

The MINOR SCALE photography was very thorough in azimuthal angle. This is fortunate due to the early wind shearing of the cloud. While not yet analyzed, untimed airborne oblique angle photographs were also taken. These will be more pertinent when the three-dimensional hydrocode outputs are being evaluated.

2.3 MISCELLANEOUS MEASUREMENTS.

The soil particles are the primary reason for the validation of the hydrocodes. The amount of particle-related data beyond the photography of particulate ensembles is limited. For the CLIMAX event, the desert surface produced a visible thermal layer before the arrival of the shock. The high SHOB of 339 ft/kT$^{1/3}$ (103 m/kT$^{1/3}$) leads to the initial Mach stem formation at the large ground range equal to the fireball edge that is well above the surface. The result is that the standard dust scouring is only significant at large ranges from the surface ground zero (SGZ). The major closer-in processes are the pore air release and the spallation from any ground shock (set up by the air shock) that reflects off of any acoustic impedance directly under the SGZ. The post shock thermal fluence on the suspended dust around the SGZ produced buoyant dusty air that was photographed.

Using parametric studies of the optical properties, the 'dust mound' over SGZ in the CLIMAX photography, seen by the fireball's illumination, can be matched by the MAZ calculations. Given the good thermal flux history from measurements and RECIPE modeling for this 61 kT airdrop, this dust mound is an implicit measurement of optical properties for the dust, once the MAZ modeling of the flux is adequate. The filmed perimeter shape of the mound may be influenced by the detailed geometry of the extended radiance source. Given this burst in darkness, neither aircraft sampling nor fallout sampling was done to provide independent PSD data for any assumed information leading to the optical properties of the dusty air region below the fireball.

In summary, the Graybeard project will address the archiving of the pertinent original fragments of information about particles. The pertinent phrases in the old Weapons Test (WT) reports that add insight are also being cataloged for future reviews.

SECTION 3

DATA REVIEW RELATED EFFORTS

3.1 OVERVIEW.

Numerous small efforts were performed that relate to the data archives. These range from reporting typos in authoritative documentation such as EM-1 and Dr. Shelton's memoirs (Shelton, 1988), to helping the Federal Aviation Authority quantitatively understand older volcanic ash cloud observations by polar orbiting weather satellites. This section will briefly discuss these efforts.

3.2 PARTIAL VALIDATION CANDIDATES.

There are frequent questions about isolated features seen in the hydrocode outputs, either for a validation case or one or more production runs. During this effort the 91-series of eight (8) initial yield and SHOB combinations were run as production cases, and then followed by an additional three for a total of 11 in the final production matrix. The stem for the surface bursts in the five production cases was seen to be quite wide relative to the early fireball. Because the Ejecta Model 4 boundary condition for MAZ is based on saturated soil cratering, we decided to look at an analog case for a qualitative validation of the relatively wide stem.

The Operation IVY/Mike surface burst event of 10,600 kT in a special two-story high device structure on saturated coral was selected as the pertinent analog. (The Operation CASTLE/Koon event occurred during a rain storm and therefore lacks any pertinent photographs; its partial misfire might also be a caveat to retain.) At our request, DASIAC located the stills for a camera that we identified was used for Operation IVY/Mike. These good contrast frames were again reviewed to confirm that the stem was relatively very narrow during the whole first minute after burst. This stem width conflict was first reported in the late 1970s after MAZ's predecessor DICE showed very wide stems for surface as well as air bursts.

Equally important to the observation of the stem size, the whole Mike stem edge was very sharp in contrast, on both the sun illuminated and shadowed sides (for the near-dawn elevation angle of the sun), and not at all diffused like the MAZ output implies from its radial dust concentration behavior. One can speculate on the optical effects of sweep-up in the dust scoured production runs versus the water sweep-up for the MIKE event. An IVY/Mike case with water was not run but the calculational outputs for all of the surface bursts were reviewed and no yield effect on the gradient was found. This apparently unsatisfactory result by MAZ occurs after a special small mixing or outer length scale was assigned just to be used in the stem region by MAZ's second order closure turbulence model (SOCTM). The net result is that the stem is possibly more complicated than the

14

approximations to date by MAZ. As advised in our previous work (Cockayne, 1993), an analog for MAZ output of the OBSCURE code used on the TASS output is recommended in order to properly process the MAZ output and avoid always relying on the steep gradient of dust concentration for implying an optically visible edge.

A model validation candidate for the soil surface region of the calculations is the periodic sweep-up tests of real dust in Australia by a team headed by Raupach. I have supplied many recent papers to the contract technical monitor (CTM) and the principal investigators for both the MAZ and TASS codes. My justification for focussing on this exo-laboratory data base is that the slow scouring speeds in these hydrocodes have a very long duration, over the blast wave loosened soil, due to the winds induced by the buoyant fireball's lift off and rise away from the ground. Thus, the newly developed sweep-up model to be used by MAZ and TASS should be thoroughly checked for its relatively major extrapolation from the Mach 0.1 to 0.3 tests over the synthetic soils in the DNA dusty wind tunnel at TRW down to the real surface scouring with Mach 0.03 wind speeds.

A new cloud rise validation candidate is the ensemble analysis for the most replicated plasma fireball in the DNA bubble rise chamber at TRW. TRW has sorted the replicates to find a few categories where many clouds followed the same chaotic trajectory through the single height cruciform of temperature probes near stabilization height. A caveat is that S-Cubed found during its analyses of these cloud rise data that the fireball has bigger asymmetries than expected from the basic engineering design and features of the DNA bubble rise chamber at TRW. (As a selling point, the TRW designers made a significant attempt to achieve a plasma burnout hemisphere in the air around the two surface electrodes.) Nevertheless, this simulator's final results provide a challenge for both the MAZ and TASS codes to match some of the ensemble features and avoid the existing issue of whether the case study comparisons are biased by major chaotic effects. This is obviously a turbulence modeling aspect and nothing will be answered clearly by this exercise. Worse yet, the standard spectral results for the TRW temperature histories can lead to the classical -5/3 frequency dependency "without the need for a self-similar cascade of eddies of varying size" (Meneveau, 1991; and a personal communication from Dr. N. Gamage, U. of Colorado on 22 September 1993). The apparent cause of this ambiguity about the presence of an eddy cascade is that spectral methods measure mainly the temporal repetitions of fluctuations, not the actual scale or any other features of the waveform deviations from the linear trend.

A new validation candidate for the period well after cloud stabilization is the endurance record setting trans-Atlantic balloon flight in September 1992 by Richard Abruzzo and Troy Bradley. The crew took frequent position readings between Bangor, Maine and the landing, 146 hrs later, about 60 mi southeast of Casablanca, Morocco. They had an onboard computer that logged the pressure altitude every four (4) minutes for the whole flight. Thus, the trajectory can be used to initiate many tests of transport codes such as SCIPUFF (second order integrated puff model), P-EARL

(Prototype Environment and Aircraft Response modeL), and NewFall. The number of meaningful trajectory tests is limited by the length, or time, to independence of the balloon positions along the trajectory. Thus, using hourly initial conditions is too frequent usually to start tests, and only initializing every ten hours gives too few tests to form any robust statistics for the miss distances of the predictions. The correct selection approach is to use a sliding autocorrelation to find the current time to independence for each wind component. This specialized processing of the validation data to prepare it for the code input and associated output comparison was not done due to the temporary delay in the P-EARL development.

3.3 ARCHIVAL ASSOCIATED ACTIVITIES.

The primary archival activity was participating in the DNA review activity for the introduction of the DNA DARE effort--Data Archival and Retrieval Enhancement. This project being performed by Caltech's Jet Propulsion Laboratory (JPL) held a workshop at the end of its first year. Because our particulate cloud review contract is one of the major users of DNA's DASIAC support, we attended the two-day workshop and offered real time suggestions for improving the design requirements for the future computerized system that JPL is evolving from an existing similar system. We also provided a follow-up letter to the JPL principal investigator for DARE and Dr. Hillendahl helped the RDA principal investigator for DARE initiate a specific archival activity.

A secondary archival activity was assembly of a nearly two hour long video tape of interesting unclassified nuclear cloud films for use at Offutt AFB by the old and new staff concerned with the various fratricide, etc. problems. This tape was sent to Sam Arwood at Offutt AFB who has a longevity of dealing with the DNA data base of nuclear cloud predictions and associated applications for the various organizations at Offutt AFB.

Another archival activity was participating in the Dust Cloud Avoidance Program (DCAP) meetings, etc. under the leadership of LtCol J. Miatech and then Dr. A. Vopatek of the DNA Weapons Effects Division. The purpose of our activity in the DCAP was to be sure that the assumptions and reference data used by the four initial DCAP projects were accurate, pertinent and representative for the dust sensor studies. This activity also involved responding to calls from the DCAP principal investigators, arranging for a gamma ray transport calculation and code approved by DNA/RARP to be used on one DCAP contract, and thoroughly critiquing the four phase one reports. The basis for this SAIC involvement in DCAP is our experience in interpreting all of the old nuclear cloud observations and in designing and applying modern sensors to use in current characterizations of simulated nuclear dust clouds.

Finally, during these two years, an effort was underway to complete a particulate cloud chapter to the (nuclear) Effects Manual (EM)-1 of the DNA. The DNA contracted publisher of that tutorial and reference material was in contact with us to clarify some of the draft inputs. We also assisted

16

them in compiling a nuclear cloud bibliography to go into the summary chapter of the EM-1. In addition, we critiqued the candidate revision or expansion of the EM-1 cratering chapter for near-surface bursts on alluvial soils. This was pertinent due to the real world ejecta source needed for the dust cloud modeling that represents other than the stressing dust loading situation that has been used to date for all the applications of the dust cloud predictions.

3.4   SPECIAL STUDY ATTEMPT.

The 1991 discovery by TASS, reported by Bacon (Bacon et al., 1992), that a strategic yield burst could trigger mission failure fratricide from gravity wave water-based clouds at many tens of kilometers away from GZ, was a major concern in the validation sense. Was there any empirical evidence of such severe 'off-site' meteorological effects? Maybe.

As background, the perceived excess of mid-USA tornadoes in the spring of 1953 lead to major Congressional hearings on the potential for the cause of the excess tornadoes being the Operation UPSHOT-KNOTHOLE series from 17 March through 4 June at the Nevada Test Site. The members of the Atomic Energy Commission (AEC) had this topic high on the agenda for many meetings of the AEC. Not unexpectedly, no one 40 years ago could find a mechanism for cause and effect; there was just the generic perceived statistical correlation. With today's knowledge, long range effects ('teleconnections') are becoming more documented by the meteorological research community, which still leaves open the possibility of some real effect. The required special circumstances (Bacon et al., 1992) of a stable tropospheric layer bounded by two unstable layers in order to produce gravity wave clouds at remote distances can conceivably have an analog for triggering tornadoes in an air mass with all of the other necessary conditions. The VORTEX Project in April-June of 1994 and 1995 is focussing on what the necessary conditions are to support tornadoes (Personal communication, H. Brooks, April 1994).

During the above effort to address the long range weather effects in 1953, the recent two large late 1952 Operation IVY bursts were investigated; I suspect that that investigation is why there are no available reports of the reduced mandatory and significant level sounding data for the King shot. While there are anecdotal reports of major unforecasted weather changes around the Enewetak Atoll, no systematic observations were made that support any analysis. (I can appreciate everyone in the meteorological support staff 'crashing' after getting each shot off given the many weather criteria for camera coverage and aircraft refueling areas.) The net result was again a need for TASS to thoroughly assess sensitivities of the prediction to the hydrocode's capability, which was done in Section 8 of the pertinent reference. [A very long shot for getting teleconnection data is that the Soviets picked up the issue and addressed it during their major testing episode later in the 1950s. How it became a null issue within the USA is not apparent from my research to date. It is possibly due to all subsequent years having significantly more observed tornadoes (Halpert et al., 1994).]

17

SECTION 4

VALIDATION RELATED EFFORTS

4.1 OVERVIEW.

Numerous small efforts were performed that relate to the validations of the modeling per se and of the predictions for the data base to be distributed by the DNA/SPWE to all interested users. These activities range from the review and revision of the cloud property uncertainties for systems level fratricide uncertainty studies in 1993, to the review of the potential effects of the automatic adaptivity algorithm in the hydrocode on the fidelity of the sensitivity studies for varying code inputs and parameterizations. This section will briefly discuss these efforts.

4.2 SUPPLEMENTAL VALIDATION SUPPORT.

There is a continuing need to have the best available quick running models of the nuclear dust clouds for sanity checks on the hydrocode outputs, and for applications that need less fidelity and more flexibility in the particulate environment predictions. Thus, the complex empirical model DELFIC (Norment, 1979), the development of which began over 30 years ago, is being updated by the doctoral thesis of Captain Vince Jodoin, USAF, at the Air Force Institute of Technology. We have helped him accurately interpret the previously unavailable upper air soundings from the codified reports in the weather data archives at Asheville, NC. We have also acted as a sounding board for his understanding of the significant shortcuts injected into the last previous version of DELFIC (Norment, 1979) at the expense of removing some first principles aspects.

While performing even a simple check on the behavior of the DELFIC predictions, we have rediscovered a simple quantitative understanding of the cause for the large stabilization altitude difference in the cloud tops ($\Delta = 8$ kft $= 2.4$ km) for two identical tower bursts of 28 kT yield and 500 ft HOB, which occurred just 10 days apart. That cause is that the Operation TEAPOT Apple-2 and Zucchini debris and dust cloud tops stabilized after traversing an identical amount of potential temperature rise beyond the prominent middle altitude knee in the profile. Associated entrainment of stable dry air is the equilibration mechanism for all large buoyant bubbles, but not for all jets.

In **Figure 4-1a**, the sensible temperature curve does not have any good visual cues or reference indicators to define the limits of a significantly stable layer for the Apple-2 event. An altitude scale was anchored arbitrarily to the U.S. Standard Atmosphere (1976) heights for the 250 and 100 mb pressures in order to be quite accurate above mean sea level for the altitude range of interest in the following discussion and comparison with the Zucchini cloud stabilization--this upper air matching causes the non-physical/anomalous altitude for the 1,000 mb level in Figures 4-1a and 4-1b.
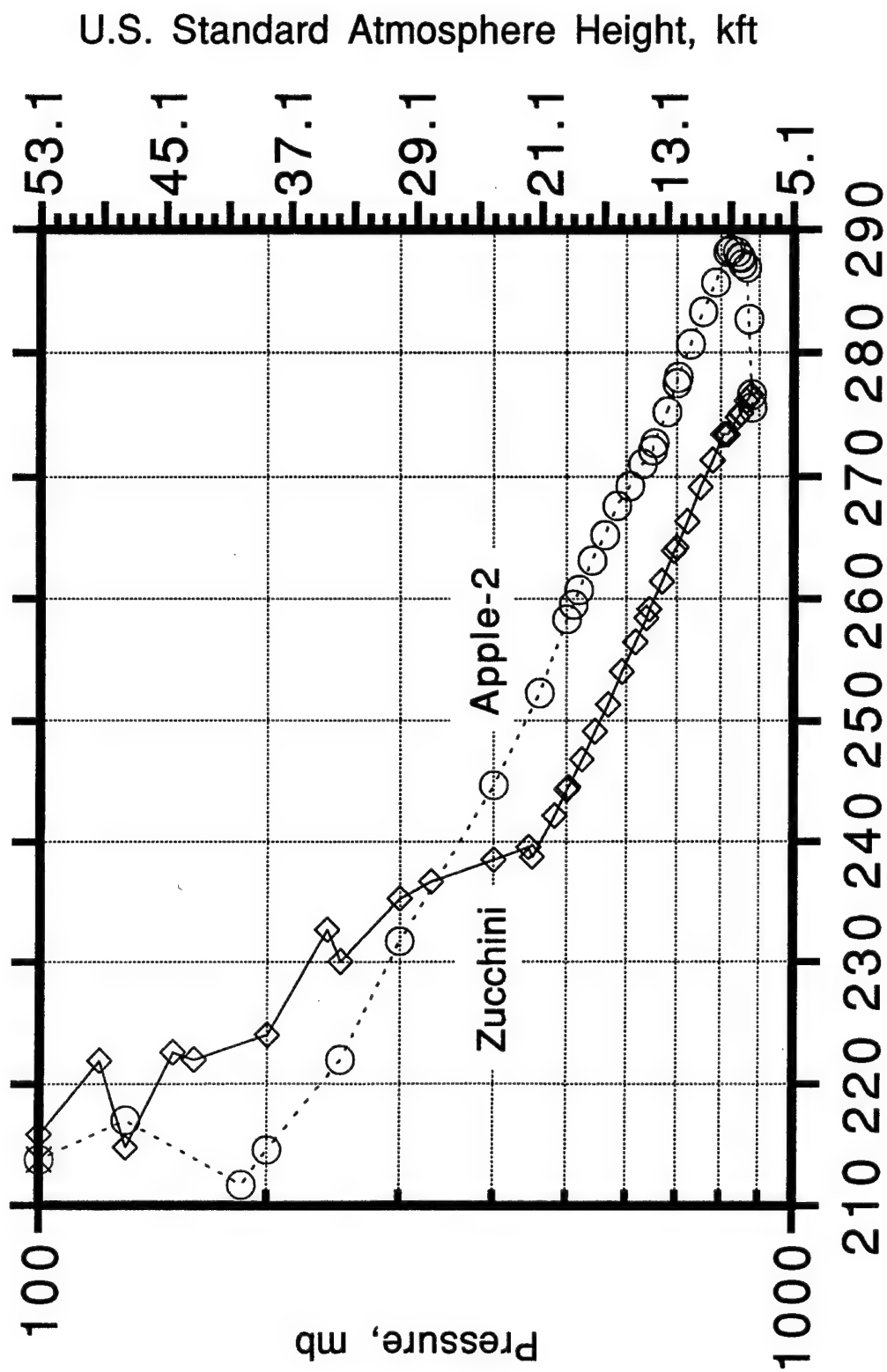
Figure 4-1a. Two temperature profiles from Operation TEAPOT.

19

In **Figure 4-1b**, the potential temperatures were formed and then normalized to the respective values at the knees near 450 mb; the depiction of an adiabatic/neutrally stable layer at 500 - 450 mb is made obvious for Apple-2 by using the potential temperature. Note the stable Apple-2 sounding section above ~450 mb, which was not obvious on the previous figure for air temperature profiles.

The Zucchini cloud top at 35 kft is apparently at the top of the temperature inversion between 240 and 250 mb. The potential temperature at that altitude is 50 K higher than the prominent knee. The U.S. Standard Atmosphere (USSA) profile is at lower levels warmer than, and at higher levels colder than, the Zucchini profile. Thus, the hypsometric equation leads to only ~1 percent error in using the right ordinate of Figure 4-1b for Zucchini's top altitude. Conversely, the USSA sounding is all colder than the Apple-2 sounding. Thus, the reported 43 kft cloud top for Apple-2 is really at the measurably lower pressure that is associated with 44 kft in the USSA sounding, which again is a change of 50 K from the prominent knee in the potential temperature profile.

An equal change of potential temperature is very significant because the 1.25 ratio of rise-distances for the two cloud tops (39 and 31 above the 4 kft ground elevation) also resulted in the tops being in the totally opposite relationship to the respective tropopause altitudes, one above and one below, which was puzzling previously. Note that the two cloud bottoms at 25 and 34 kft are also in good agreement with each other based on this technique of matched changes in potential temperatures. The hypsometric equation results for the Zucchini sounding lead to the reported 25 kft bottom being 2 kft above the 400 mb level--the linear right ordinate already has a 1 kft bias at that height. The ~16 to 18 K temperature rises from the two pertinent knees are very consistent. Both clouds were non-reactive because they did not experience any buoyancy perturbation from a significant latent heat release by entrained moisture. Thus, a stabilization simplification can not be generalized, but it is very pertinent to the large variability in the cloud tops for the kiloton and sub-kiloton bursts that normally do not rise far enough to have significant heat release by entrained moisture. This simplification is especially good when the time of day is considered, such as for TEAPOT/Ess occurring near noon on a clear day with a neutral temperature lapse rate for most of its rise.

Another meteorological aspect for modeling validation is the extrapolation of the winds from the 850 mb level (~1.5 km above mean sea level--MSL) down to the surface. In the Fratricide Prediction Model (FPM), a generic profile is used for the large downward extrapolation. This profile, which is always applied in the FPM, is theoretically possible, but generally a gross approximation due to the normal planetary boundary layer (PBL) partially decoupling the terrain and surface from the free troposphere. Thus, the surface wind velocity correction is only a minor improvement over not making the correction in the few cases when it does work well. Due to the negligible sensitivity of fratricide for reentry bodies/vehicles to this fix, there is no negative consequence. However, any use of the FPM methodology for an aircraft flight at an altitude low in the PBL is more likely to have the wrong wind velocity modification than the right correction.
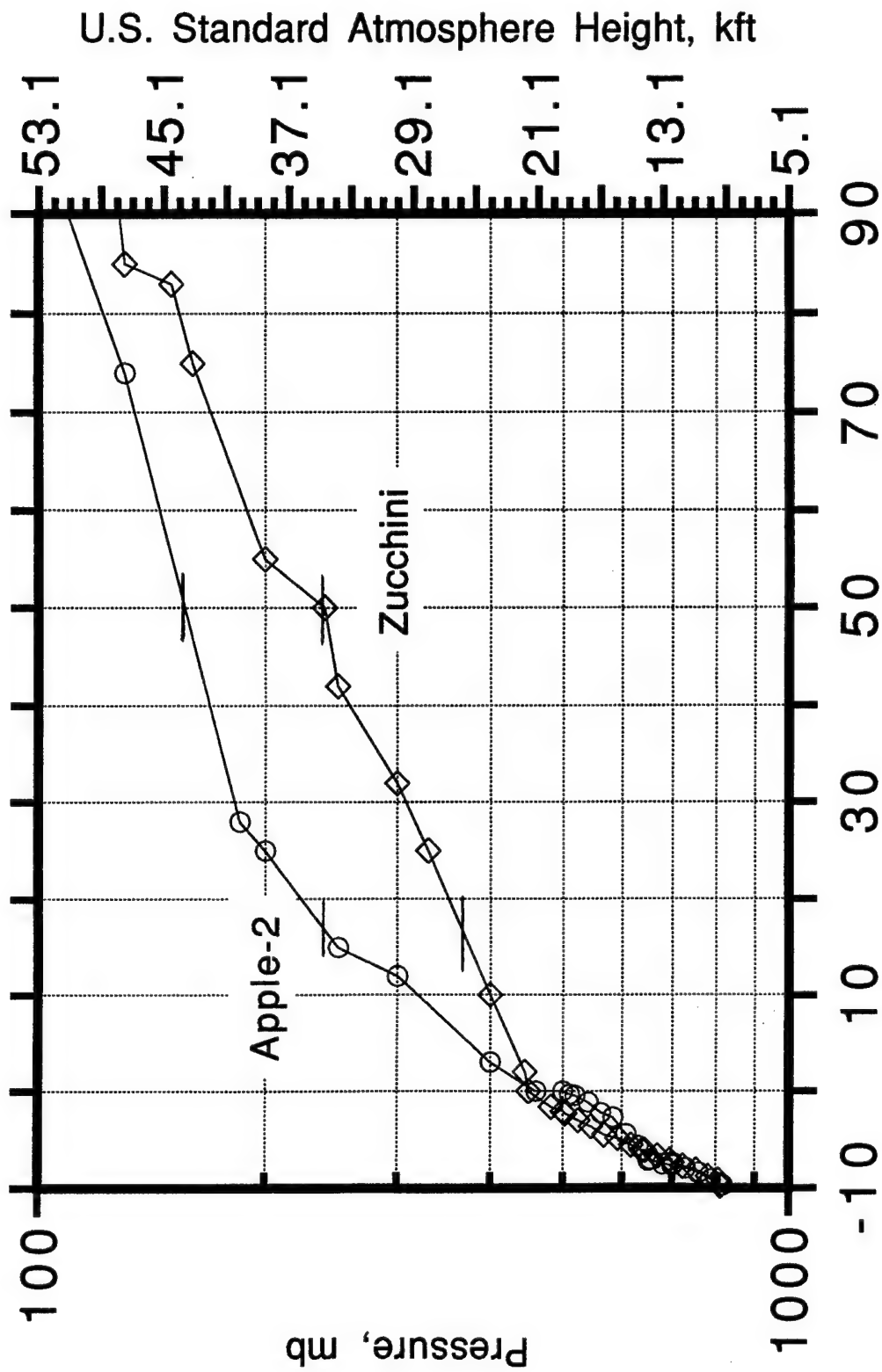
Figure 4-1b.   Profiles of the potential temperature change from the potential temperature at the respective knees near 450 mbar at a middle altitude.

4.3 HYDROCODE OUTPUT VALIDATION EFFORTS.

There is an explicit need to thoroughly review the MAZ and TASS code outputs before they are applied to critical response predictions. The first effort on this topic was the preparation of P-EARL initial conditions from the whole 91-series data base of MAZ and TASS outputs. The stressing aspect of this transform is that many more size tracers are needed for each of the seven sub-millimeter diameter fluid tracers in the TASS outputs; 50 total tracer sizes is not atypical. This transform from TASS outputs to the inputs for the P-EARL code was performed in early 1992 at SAIC/McLean using the essential subroutines of the Dial-A-Cloud (DIALACLD) code. Subsequently, the upgraded DIALACLD code was sent back to Dr. J. Stoddard for significant subsequent upgrading in order to support the FPM applications when run by personnel that did not know anything about the subtle sensitivities in the 91-series data base.

The DIALACLD upgrade by Stoddard was supported by our own critical cross comparisons among the cases within the 91 series. Numerous analyses were performed and the results circulated using almost weekly memoranda with attached figures that addressed the scaling issues and apparent inconsistencies. The net result was uncovering a complex behavior in size space for the pebbles airborne above 2 km at stabilization time. In addition, a TOSAC code error found by Dr. Stoddard in the water/snow conversion to hail equivalent sizes and mass concentrations for FPM applications was verified independently.

The most significant output discovery was the variability in the PSDs of the pebbles with yield. This PSD feature surprise was verified with an additional case calculated by MAZ and TASS. The consequence was that the uncertainty for the PSD around the largest airborne sizes was increased in the input for the major FPM investigation of all the environment and response uncertainties.

Finally, a pseudo-validation of the SCIPUFF and P-EARL codes was arranged among the other contractors and summarized. This used the so-called "dust-off" approach of having those late-time codes run a suite of sample single and multiple problems for the same wind fields. The predictions for the dispersing clouds were analyzed extensively for global features by using (a) standard statistics from linear regressions, with weighting by the local mass concentration, to characterize the 'puff' positions and orientations; and (b) statistics with an inversion of the non-zero mass concentrations in order to highlight any gap, void or virtual valley in the spatial distribution for any altitude. Thus, the two complementary sets of statistics provided information on the cloud centroid location, its latitudinal and longitudinal spreads, the mean azimuth of an approximate linear cloud, the angular spread around that mean azimuth, the average particle size, and a standard deviation of the size.

4.4 REVIEW OF MODELING ISSUES.

The modeling challenge is to obtain a closed suite of compatible, credible and confirmable parameterizations for the many multi-scale processes that are the significant sources and sinks in the four/five coupled conservation equations for each of the various masses of gases, liquids and solids. Among the major exchanges that are parameterized are the diffusivity, or so-called turbulence effects, and the thermal radiation loss from the fireball and photon absorption by pertinent dust particles. To date the developments have focussed more on relatively fast running parameterizations that achieve closure versus on absolute accuracy over the complete dynamic ranges of the algorithms inputs and outputs. Thus, a constant small effort was directed to finding updated parameterizations and validated data sets in the multi-phase fluid dynamics literature that are pertinent to this cloud problem.

The large lack of empirical knowledge about the probable hybrid water/ice and dust particles is one potentially significant shortcoming of the MAZ and TASS modeling. Even for regions without mud particles appearing on the windscreen of the sampling aircraft, the PSD predictions are approximate. For example, a factor of over 30 between the mass mean diameter for a stem sampling pass (7 min) at the MINOR SCALE shot and its post-shot 'prediction' was not addressed directly during this two year effort. However, implicitly, an approximate factor of 30 was decomposed into (1) an instrument bias by a maximum factor of 3 (i.e., the sensed area is <u>always</u> high by a factor of the order of 10, which both covers all of the glint possibilities and assumes that every particle causes such specular scattering) and (2) a calculational bias by a factor of 10 for those dust diameters that <u>approach</u> the size at the predicted peak of the PSD for this experiment. This factor of 10 around a 10 μm dust diameter leads to the factor of 15 bias for 1 μm diameter dust that was used in the ongoing DNA Fratricide Prediction Model investigation by SAIC of the strategic launcher/reentry missile erosion/penetration response to the dust/pebbles (Stoddard, 1994).

The exploratory efforts by both hydrocodes have shown sensitivity to the particle-particle interactions. The resulting uncertainty in the PSD has been partially propagated into the dust, etc., response calculations by using a factor of 15 decrease and increase around the minimum 1 μm diameter dust size, and a factor of three (3) around 1 cm. Because of the sub-meter scale equilibration distances for the smaller sizes in this range, their locations out to times of less than one hour after burst are assumed to be unaffected to first order by such large size shifting for response sensitivity studies. Thereafter, the significant settling speed differences do have an altitude impact for such simple size uncertainty investigations. The net result is that the PSD variability and uncertainty for each soil texture and embedded water class is still a challenge for good modeling and other confidence building steps.

23

Finally, the additional fidelity of the numerics from locally adapting the cell spacing is also more code complexity that needs evaluation. Per se, grid refinement is good because it can help computational convergence assuming that every parameterizations is well behaved while being used simultaneously at all the grids sizes, which can easily vary in area by over a factor of 16,000 for just 8 m to 1,024 m grid spacings by seven steps of a factor of two. In shock hydrocodes, such significant size ranges imply much more numerical diffusion in all large cells unless the time steps are also locally changed in proportion to the cell spacing. In any case, all solutions tend toward an attractor for varying inputs because the adaptivity algorithm interacts significantly with the solution, unless the only changes are the boundary conditions. The net result is that the sensitivity studies for varying inputs must compensate by such schemes as using the same refinement history in both runs, which is analogous to the one series of random numbers being used for each Monte Carlo code sensitivity study.

SECTION 5

THE MUDCAT PROJECT

5.1 INTRODUCTION.

Numerous dust and other non-natural clouds are important enough to be modeled so the predicted particulate data can be used in subsequent calculations. Two implicit requirements at this time are obtained from the following situations and motivations.

Natural water-based clouds have particulate albedos of almost 1.0 for solar radiation and therefore nearly negligible insolation heating of the cloud. Excluding steam releases, most other clouds contain lower albedo particles. Important examples are dust storms and large air pollution sources. Thus they have significant insolation heating when the clouds are large enough along the sun beam to have an absorption optical depth over about 0.1. That is, about 100 W/m^2, or order of 100 kcal/m^2-hr, of radiative heating is in the particulate-laden air rather than heating/hitting the surface. Because such optically thick clouds may remain compact for the order of an hour or more before visible dilution, they have a heating supplemented dispersion until they are actually a passive additive in the ambient atmosphere. Such optically active clouds are a select subset of all air pollution clouds, but they include all bomb bursts.

The world's largest visible, and perhaps ugliest, pollution cloud was the soot, oil droplets, salt, etc. particulate plume from the oil/gas field fires in Kuwait from late February to early November 1991. The DNA and others jointly sponsored intensive data observations of that plume in late May and early June 1991. One purpose of that effort was the modeling of the turbulent transport in the free troposphere above the planetary boundary layer (PBL). The motivation was that there is large variability in the effective diffusion rate, during even the horizontal dispersion, at all times after parcel release. The sampling replication in different daily wind fields over and around Kuwait held the promise of enough data to formulate a basic empirical model of the variability in the effective horizontal diffusion rate versus time after parcel release. The tentative results were that a newly documented paradigm potentially dominated the co-altitude growth of the plume width. The insolation heating of the plume produced strong enough vertical motions that the directional wind shear (along the vertical axis) lead to a sunny side growth of the adjacent higher layer in the plume.

A hypothesis from the tentative results is that minimal co-altitude, or horizontal, growth occurs for NBC (nuclear, biological and chemical) clouds in the free troposphere with stable soundings, unless there is significant sunlight absorption. The stable sounding condition varies by season and location from above to below 50 percent of the time. The conditionally unstable sounding conditions will mostly be included in the stable sounding condition due to the significant height rise required to trigger free troposphere condensation. To verify this understanding for the puff type clouds in addition to the plume type cloud, a DNA project was formulated to observe the diffusion

in the first few hours after the kilometer scale dust cloud was injected by the MINOR UNCLE HE event; which was the MINOR UNCLE Dust Cloud Atmospheric Transport (**MUDCAT**) project.

The second motivation for the MUDCAT project came from a renewed concern about the prediction of volcanic ash hazards. In September 1992, the southern Alaskan Mt. Spurr volcano emitted ash (and gases) that some weather satellites still saw as a contiguous plume when it entered the air space controlled by the Cleveland Air Traffic Control Center nearly two days later. Lacking even any approximate ash mass concentration calculations either directly or by processing the multi-wavelength imagery, the pilots and flight routers of all airlines deviated well away from the likely location in order to avoid any damage to the engines, windscreens and other vulnerable items. There was a major cost/consequence and some impact on the air traffic may have been simply excess concern in the absence of any concentration indications. MUDCAT also had the potential to obtain the same weather satellite data for a characterized cloud of soil particles.

The specifics of the MINOR UNCLE event are the following:
-   2,400 tons of ANFO[4] HE (an airblast equivalent to a 4 kT nuclear surface burst)
-   a crater volume large enough to supply tons of small/sub-microgram dust
-   a virtually cloud free sky that permitted unambiguous satellite imagery
-   an empirical cloud top rise to 4.5 km (15 kft) above ground level[5]
-   an early morning shot time that permitted subsequent satellite scanning.

The assets needed to conduct the MUDCAT project were all existing operational capabilities that SAIC was familiar with in some manner or the other. The National Center for Atmospheric Research (NCAR) maintains a large Research Aviation Facility (RAF) that has a turbo-prop (King Air) aircraft equipped for pollution studies of particles and gases, which was available if the scheduled date of 10 June was maintained. The digital satellite images could be received and recorded at the Weather Support facility on the main post of the White Sands Missile Range (WSMR), on a non-interference basis, and likewise at the University of Colorado. The Los Alamos National Laboratory had an in situ sampling project in the first hour to obtain filters for dust particle characterizations, which would provide some indication of an earlier cloud width at altitudes repeatedly sampled later. Finally, WSMR's documentary photography had large format cameras for high resolution images with wide fields of view at the time of satellite imaging.

The rest of this section addresses the various data collections and analyses to date that can be used in subsequent dust cloud diffusion modeling studies. This summary complements the full report presented in separate reporting for the MINOR UNCLE event (Cockayne and Edwards, 1994). The tireless efforts of the NCAR/RAF staff are appreciated for fielding the sensors and recorders as well as explaining the nuances of various signal records; specifically, the program manager, Mr. Bruce Morley, the sampling system operator and atmospheric chemist, Dr. Greg Kok, and the particulate probe expert, Dr. Darrel Baumgardner.

---

[4] Ammonium Nitrate with 6% Fuel Oil.

[5] Mr. Paul Hassig of CRT supplied a MAZ prediction for an assumed nominal sounding.

5.2 UPPER AIR SOUNDINGS.

Numerous upper air soundings were obtained before, 'at' and after the shot time, including those during the climb well after the burst to the cloud top by the NCAR sampling aircraft. The local standard 'roabs' with readouts of the rawinsonde data are the following (the 1200 UTC profiles at MDT = 0600 for Albuquerque and El Paso are also available for ~100 nmi away):

Release Time	UTC	MDT	Location
H-6 hrs	0906	0306	Admin Park
H-4.67	1030	0430	Admin Park
H-2	1310	0710	Admin Park
H-1	1405	0805	Admin Park
T=0	~1510	~0910	Admin Park, Stallion Gate and Jallen
H+2- hrs	1702	1102	Admin Park

The thin layer/'knee' of quite stable air (isothermal air temperature) near 525-520 mb was where most of the upper dust cloud top stabilized; it was the interface of an elevated front up into virtually warmer air that was also 20 °C drier in dew point near the interface. The cloud top portion initially entrained a significant mass fraction of its air above the 825 mb level (top of the cool PBL over the warm surface layer) and thus the top stabilized with only about a 10°C change in potential temperature. (For a comparison, the two Operation TEAPOT events of Apple-2 and Zucchini with 28 kT yields on 500 ft towers both had a 50°C change for their cloud top stabilization from a relatively 'high' airburst with minimal dust mass (Cockayne, 1994).) The relatively moist parcels entrained around 600 mb could just achieve saturation, by following their mixing ratio line to the 525 mb knee and excluding any mixing dilution. The net result is that the only possible water/ice particles in the cloud came from condensation of the ANFO by-products.

There was nearly a light and variable wind category throughout the cloud height of notably less than the 7 km-MSL as predicted by MAZ for a nominal sounding. The net result was that the cloud stayed within the WSMR but was in many fragments beyond ten minutes after burst, due to the accompanying directional shear with height. The air inhomogeneities are also evident in the potential temperature profiles encountered by the sampling aircraft during the transit down to WSMR from Albuquerque, the climb to the Flight Level (FL) 175[6] sampling around the 5,300 m-MSL **pressure** altitude, the climb on up to the cloud top, and the descent down to the hour of sampling near FL 100, which is 10,000 ft-MSL pressure altitude (3,280 m) and also about 750 ft higher[6] than 10,000 ft. To complete the upper air understanding, a suggestion is to obtain the temperature profiles from the TIROS Operational Vertical Sounder (TOVS) on the pertinent passes of the orbiting NOAA satellites. Then, the empirical upper air data set could be much more

---

[6] For the conditions following the shot time, the pertinent 516.5 mb in the Standard Atmosphere for the 17.5 kft geopotential altitude (gpa) was up at 18,228 ft-MSL, and the 696.8 mb for 10 kft-gpa was at 10,444 ft-MSL.

27

complete for validating either the simple SCIPUFF and P-EARL codes or the first principles based OMEGA and MEDOC cloud translation and diffusion codes.

5.3 TIME SERIES.

Numerous variables are available from the computerized data acquisition system on the NCAR aircraft. Only some of the ~250 channels address items that are pertinent to the diffusional behavior of the puff cloud. Some of the following are presented mainly for an orientation to the data base and sampling flight patterns. The flight pattern was essentially a figure eight loop that rotated in azimuth and produced a so-called wagon wheel effect from the total passes, which will be shown in the next section. The preliminary pass times for the wagon wheel of ten passes at FL 175 are:

Pass No.	Start Time, UTC	Stop Time	Duration (sec)
1	153900 (15.65)	154210 (15.7028)	190
2	154505 (15.7514)	154610 (15.7694)	65
3	154805 (15.8014)	154855 (15.8153)	50
4	155000 (15.8333)	155135 (15.8597)	95
5	155303 (15.8842)	155450 (15.9139)	107
6	155550 (15.9306)	155649 (15.9469)	59
7	155800 (15.9667)	155920 (15.9889)	80
8	160045 (16.0125)	160200 (16.0333)	75
9	160240 (16.0444)	160455 (16.0819)	135
10	160600 (16.10)	160715 (16.1208)	75

Figures 5-1 and **5-2** show the air temperature histories every second and also after a triangular filter smoothing using 11 total points (9 non-zero), which is about an 8 sec (the order of 800 m) effective width (Blackman and Tukey, 1959). The approximate in-dust-cloud times are the ten (10) thick horizontal bars along the top of the plot. In actuality, the first pass was 250 ft lower than the other/last nine so its cold temperature bias is especially noteworthy because it should be a warm bias. It is doubtful that that spatially separate portion of the cloud was in a gravity wave effect where adiabatically cooled ascending air (-1.5°C from co-altitude air) was being sampled.

Figure 5-2 compared to Figure 5-1 implies that there are significant sub-km scale inhomogeneities, such as in pass 2 around 15.76 hr UTC. Nevertheless most of the variance is in larger lengths, given the nominal true air speed of 100 m/sec and thus 18 km per time grid line. A wavelet or other phase plane analysis may be better than a standard spectral analysis of the air property variance, for characterizing the so-called clear air turbulence, due to the changing pass locations relative to the puff center and the associated effect on the characteristic length and its spatial distribution.
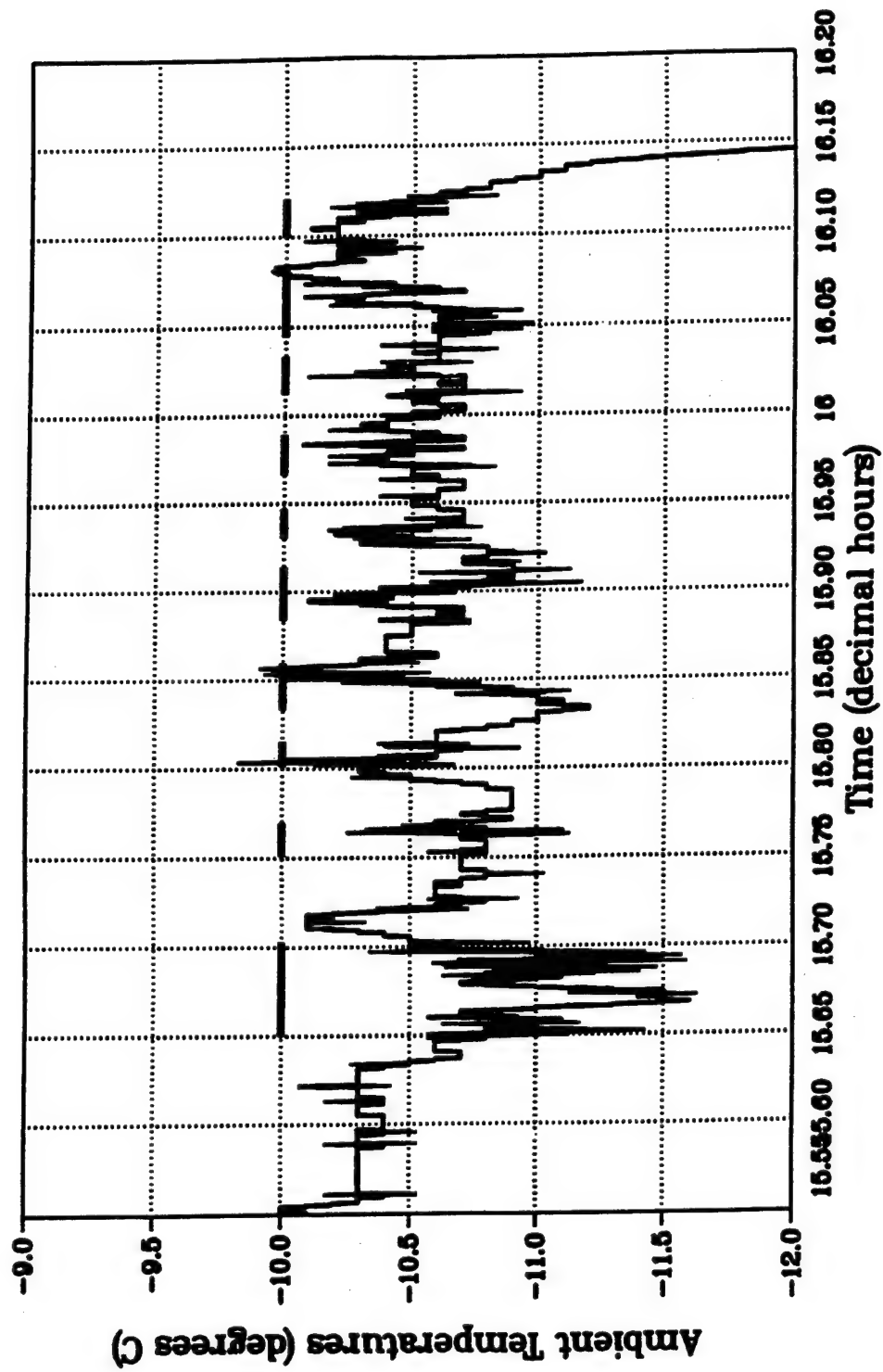
28

Figure 5-1. Air temperature every second for sampling at FL 175; and bars for 10 passes.
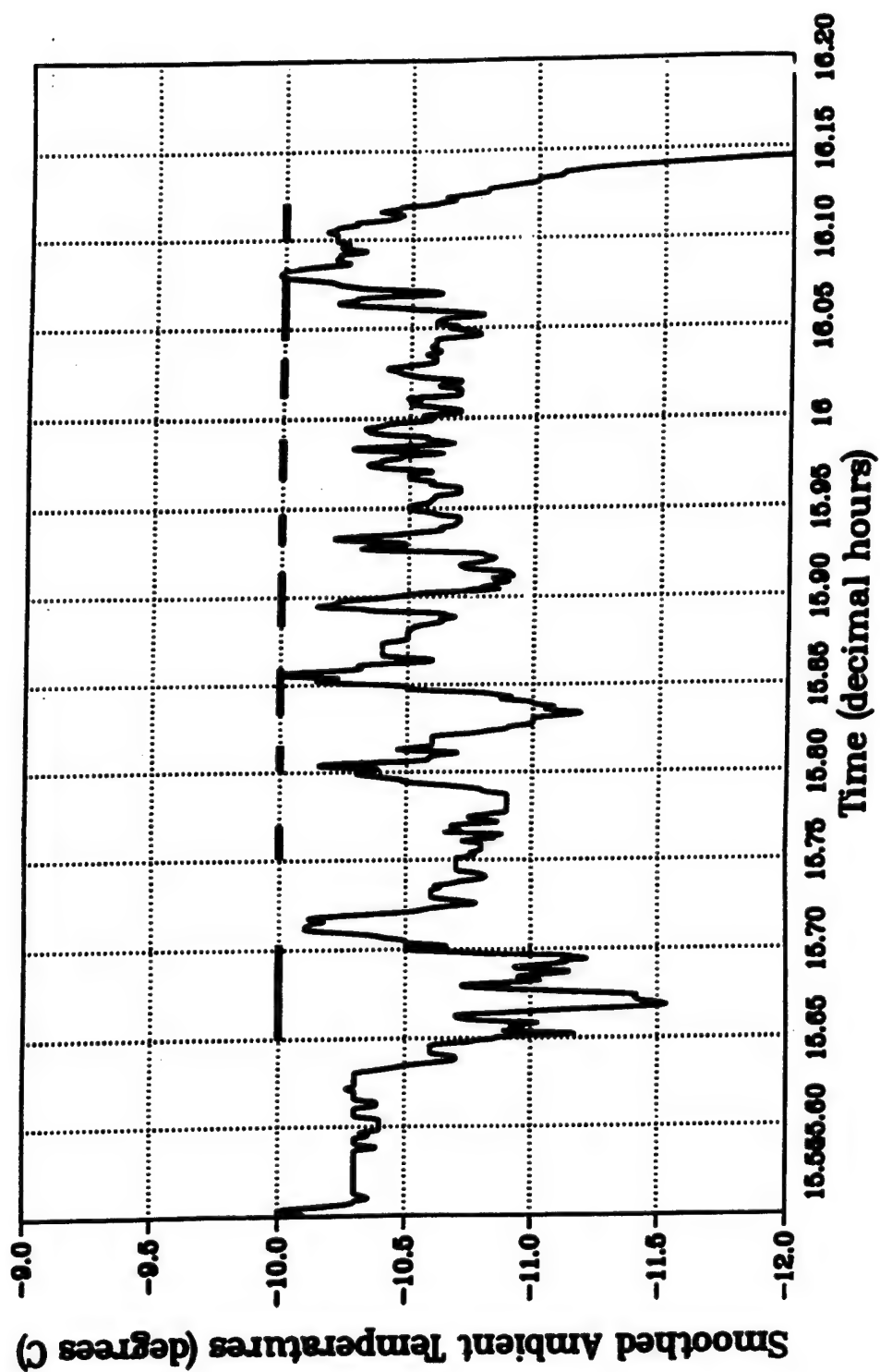
29

Figure 5-2. Air temperature every second after a 11-sec wide triangle weight filtering for sampling at FL 175; and bars for 10 passes.

30

Figure 5-3 shows the digital-counts record at FL 175 for an ANFO by-product (the oxides of nitrogen, NO_y), except for pass two (15.75-15.77) where the sensor was off-line for calibration checking at these high concentrations. The notable aspect of these penetration traces is the lack of diffusive leading edges, even after the intensive in-cloud turbulence at stabilization time has performed its mixing effects as it is dissipated. See Cockayne and Edwards (1994) for a detailed diagnosis and discussion of the gradients for the 18 edges. The bimodal stairstep of pass 5 around 15.9 hrs is verified by pass 9 on the reverse heading about 10 min later; see the map in the next section. The CO measurements plot is not shown due to its zero-offset and frequent absence (passes 2 and 7-9) due to the sensor zeroing by the operator. However, the 'pulse' in each pass has a different character than the NO_y pulse. Nevertheless, there is a consistent indication of peaks still over 1 ppm even after 2,000-3,000 sec of turbulent flow with its associated mixing and dilution.

The net result is that there are many variables for defining an intensity weighted distance variance for each pass, which is what NCAR did for the Kuwait plume passes (Cooper, 1994). There is general, but not exact, agreement on the locations of the cloud edges for the different puff tracers, excluding the vertical gust. There are frequent fast jumps by a factor of two in the particulate concentrations that are confirmed by the other particulate probes' simultaneous behavior.

5.4 MAPS OR SNAPSHOTS.

Numerous passes at the same altitude permit forming a crude contour map by just plotting the measurements where the aircraft flew. A meaningful map occurs when all of the observations are calculationally translated by an ambient wind to the locations at one common time, for example, the mid-point of the sampling time at the FL 175, which is 1555 UTC (15.9166). Fortunately, this time also nearly corresponds to when the satellite imaged the cloud, which is ~1557 UTC. This section will show some sample plots of various parameters constructed in this fashion.

Figure 5-4 shows the coded air temperatures within this 5 nmi by 6.7 nmi rectangle, which has the same scale in both directions. The earlier listed preliminary pass times provide the masking for only showing readings that are in the cloud. The air temperatures were averaged over three seconds in order to declutter this map. These data are after horizontally translating each temperature to the snapshot time of 1555 UTC. The time translation used the (changing) wind at the current aircraft location for each second of time adjustment, either forward or backward to the 1555 UTC, so each pass has contiguous samples and all are slightly shifted from their proper positions.

One thing to notice about the wagon wheel is that by using approximately a 225° turn, each sequential pair produces a net 90° turn so that (nearly) orthogonal passes occur every second-later pass. Figure 5-4 includes the pass number at the start of each pass for identification. The special background NCAR pilots maintained this turning procedure so well that there are essentially only four sampling directions, which do differ from their opposite heading for the fourth-later pass.

31

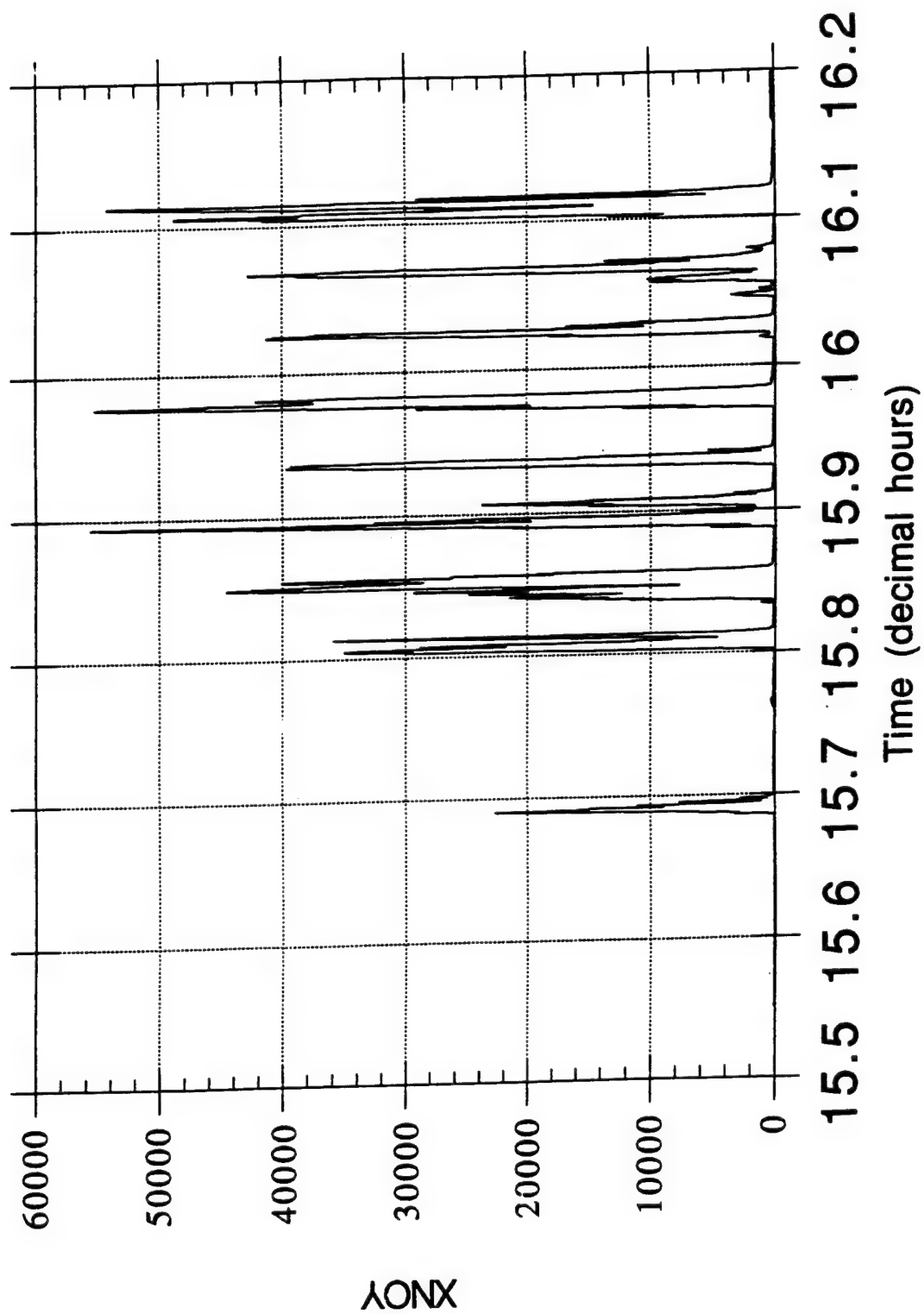Figure 5-3. Oxides of nitrogen every second, excluding pass 2, for sampling at FL 175.
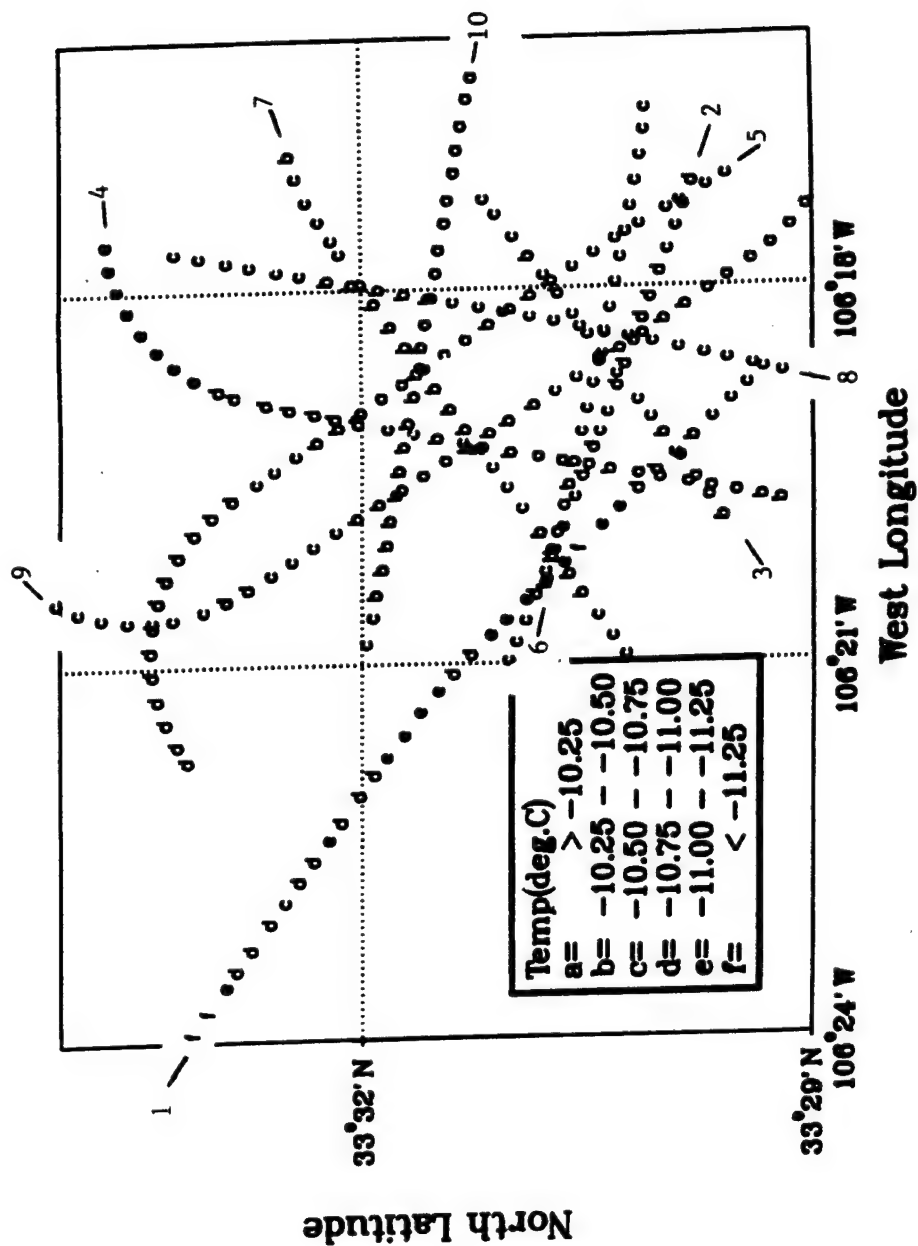
Figure 5-4. Air temperatures and horizontal winds averaged over three seconds and each temperature plotted at the position determined by the history of aircraft-encountered winds between 1555 UTC and the respective observation time for the 10 passes during sampling at FL 175. Each pass start point is labelled by the pass number.

33

The air temperatures in the snapshot are not as consistent as expected. There are intersections where the values differ by over one bin; that is, >0.25°C, which could be up to 0.75°C maximum. Nevertheless, excluding the colder pass 1 at about a 80 m lower altitude (see Figure 5-2), many intersections do agree even without invoking the pertinent uncertainties by knowing the two or more local standard deviations both for the temperature and especially for the position.

The Cockayne and Edwards (1994) report shows the ozone map expected at 1555 UTC (15.9166 hrs) as an indicator of whether the SAIC-defined pass ends went far enough to reach the pertinent ambient value.[7] This criterion is used because ozone quite quickly diffuses horizontally into a depleted region and restores the pertinent background level (unless NO is still present near the cloud surface to cause reactions that use up some ozone). There are pass ends without the code letter 'a' for return to the background level and thus some extension of the pass times is justified.

Figure 5-5 shows the time adjusted data for the dust population between ~3 and 80 μm diameter, with blanks for some sets of three consecutive zeroes but no other elimination criterion such as the time masking used above. Bootstrapping from the previous maps, one can connect the various passes and extend pass 10 for another 5 min out to the west, where the aircraft made a climbing turn to prepare for a sample of the higher cloud fragment. (Presumably dust is in the tubing to the PCASP and causing an artifact in defining all the pass ends.) The plot is somewhat deceiving due to the fact that the latest observation is plotted over any previous value(s). (Perfect positioning would permit magnifying the plot by two times in order to declutter the cloud center and the symbols could be made smaller too without losing the pass perspective and needing to stop the three second smoothing.) Nevertheless, there is general consistency, despite the position errors from the imperfect translation technique. The number density down near FL 100 has a different geometry of the pattern for the region where some special sensor studies were being performed by another experimenter flying well outside of the cloud.

5.5 SCATTER PLOTS.

A dust cloud can be characterized by several variables. In this section, the gases and smallest particles will be used to contrast the FL 175 and FL 100 regions, which are the regions of the cloud top and bottom, respectively.

Figure 5-6 is a concentration scatter plot of the condensation nuclei (CN) versus the oxides of nitrogen (NO_y) for the FL 175 samples both in and out of the visible cloud. These tracers of standard pollution are also available from the ANFO by-products' condensation and chemical reactions, respectively. Most of the 1-sec values are (very nonlinearly) correlated to increase

---

[7] Dr. Kok, NCAR sampling system operator, indicates that the values are about 25 percent too high.
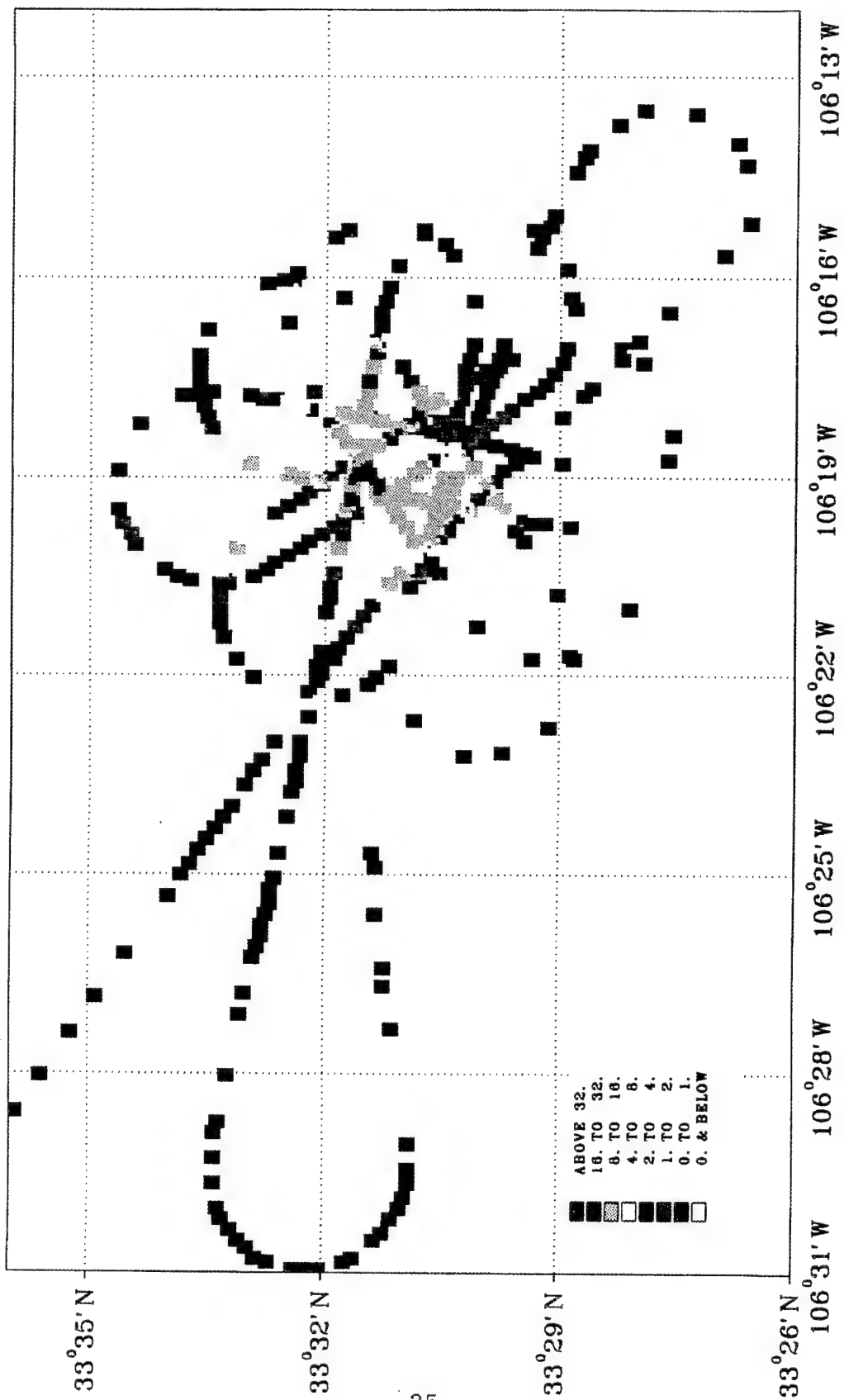
Figure 5-5. FSSP-100 particle populations (#/cc) and horizontal winds averaged over three seconds and then plotted as for Figure 5-4 during all the time of flight between 15.55 and 16.2 hr (UTC) or about FL 172 and FL 180.
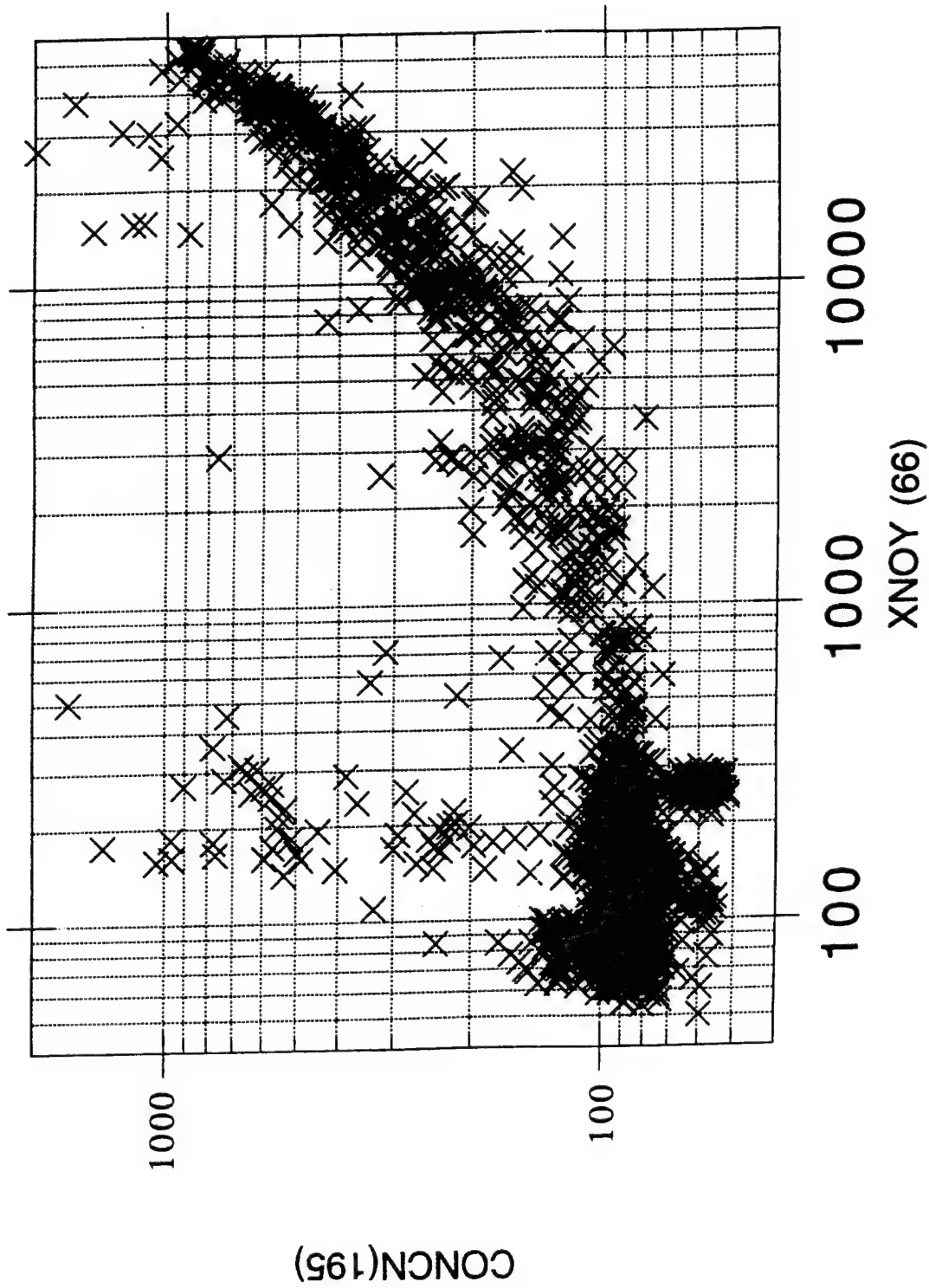
35

Figure 5-6. Scatter plot of one second values for CN and NOy during all flight between 15.55 and 16.2 hrs (UTC) or about FL 172 and FL 180.

together over background values. About 50 points have high CN readings without corresponding high readings of NO_y. Other correlations trace the gas dynamics for the reactive species. For the companion to Figure 5-6 for FL 100, there is practically no correlation of the CN to the lower amount of NO_y that is in the FL 100 layer. This drastic difference suggests that the NO reacts on the surface of the massive ejecta volume as it enters the fireball, in preference to being transformed into the NO_y gas once it mixes with air with its inherent ozone. This suggested concept clearly leads to early differences between the initial fireball 'top' and 'bottom' as distinctly divided by the highest angle 'ray' of ejecta originating from outside of the charge container. Note that Dr. R. Henny at Field Command DNA has highlighted his finding of grayish colored pebbles. He has also seen a light coloration in the Robbie Williamson photographs of the continuous fallout in the downwind direction. He has seen these phenomena for both the MINOR UNCLE and DISTANT IMAGE events. (I saw light gray colored pebble fallout from MINOR SCALE almost 1 km downwind.) In addition to the effect on the NO_y, there are fewer high CN values over ~500 per cm^3 in the FL 100 data, consistent with a dust and pebble scavenging behavior in the ANFO fireball portion that has a massive injection of soil.

5.6   TIME CORRELATIONS--AUTO AND CROSS.

Numerous methods are used to obtain inhomogeneity indicators. A spectral approach like the (fast) Fourier transform (FFT) or the maximum entropy method (MEM) is standard for those steady state problems with randomly repeating deviations. A spectral approach focuses only on frequencies, not durations, of the fluctuations that dominate the variations in all assumed nonstop processes. A consequence of this focus on frequency is the total loss of any indication of the shifts at different times in primary frequency. The inherent spectral leakage or smoothing of the FFT technique leads to a preference for the MEM when the variance is in separated bands. This preference is true whether or not the band variances are simultaneous at any time that is included in the transform window. This independent band behavior dominates all the atmospheric mixing that does not cascade each eddy to a next-size-down eddy. Such multiple band variance was observed in most measurements of the smoke plume downwind of Kuwait (Personal communication, Dr. A. Cooper, Sept. 1993). Nevertheless, the spectral variance is a common variance summary form.

An intermediate step in finding a Fourier spectrum is obtaining the autocovariance function, which is the lagged inner product of the time series. (This function is weighted by a specific frequency cosine wave to obtain the Fourier variance at that frequency.) For understanding the non-steady state or non-repeating processes, the autocovariance can be normalized to its zero-lag value in order to define the autocorrelation function. That was done in Cockayne and Edwards (1994) in order to estimate an average time scale for the pulses forming the passes in the long sampling records at FLs 175 and 100. Likewise it is applied to the ambient air properties as a method of estimating the inhomogeneity scale size.

37

Figure 5-7 shows the wind speed's autocorrelation function for 15.7166... UTC (154300) to 16.12 hrs (160712), when the flight was presumably within the identical layer of air. An e-folding decay time (distance) is on the order of 40 sec (4 km), while there is a significant correlation with ~3 and ~8 min later observations. The 40 sec e-folding interval also exists in the wind direction's autocorrelation but it has a prominent ~4 min peak that could confirm the relative peak at the same delay time on Figure 5-7, and also confirm a potential harmonic on both plots at ~8 min of delay. Because the sampling pattern has no repetition cycle around this period, there is the possibility that this is a real wind wave moving through the cloud region with a ~4 min period, which is a nominal value of the Brunt-Vaisalla frequency for the upper atmosphere (the square root of 'g_0' times the vertical derivative of the natural logarithm of the potential temperature). Given that a 0.7 correlation leads to a 49 % coefficient of determination, we see that this (implied) subjective small scale length definition produces values from 1 to ~1.7 km.

For the vertical gust's correlation, the e-folding time is much shorter. Likewise, the correlation for an independent vertical velocity estimate is shorter than for the fast horizontal wind variations. The air temperature's correlation has the same e-folding time as the horizontal wind data but the correlation is unlike any prior plots at longer delay times for this time block (nine passes/eight turns in the air mass at FL 175). Thus, the variations in the air properties are apparently not from a mutual mechanism driving the variations, or at least the deviations are not responding with the same time constants. This leaves open the potential that the sun's insolation heating is active and significant.

There is a high temperature correlation at ~13 min (780 sec) of delay. This matchup is passes 2-5 correlating with passes 7-10, considering the different averages over 673 sec in forming the 673 deviations for the inner product sum. This high number of deviations leads to a three-sigma significance[8] for each correlation function value over 0.12. It is doubtful that the peak 'r' value is high enough to justify a serious interest. If anything is buried in the long time correlations, the four replications of ~600 sec between pairs of parallel passes is the information to go after in the sense of a Lagrangian time; reversing the time axis is needed due to the reversed sampling direction.

Figure 5-8 shows a cross-correlation with the asymmetric behavior of the vertical wind lagging the ozone for just the in-cloud times at FL 175, which are all somewhat longer than listed earlier. The 1 to 15 seconds of values lower than the baseline of -1 is interpreted as the air with the significantly higher ozone loading going downward after the initial negative motion, and vice versa for a negative ozone deviation times a positive vertical wind. Given the known negative ozone deviations in the cloud, it suggests a systematic upflow bias from the long term vertical wind average. So little time was 'wasted' on any exo-cloud flying that it will be hard to understand if the bias is in the background flow or cloud heating induced.

---

[8] This peak long time air temperature autocorrelation of ~0.39 is ~10 sigma; 0.12 = 3 over square root of 673 is Saaty's significance test (Saaty, 1988) (Personal communication, Dr. Harvey Singer, 22 September 1993).
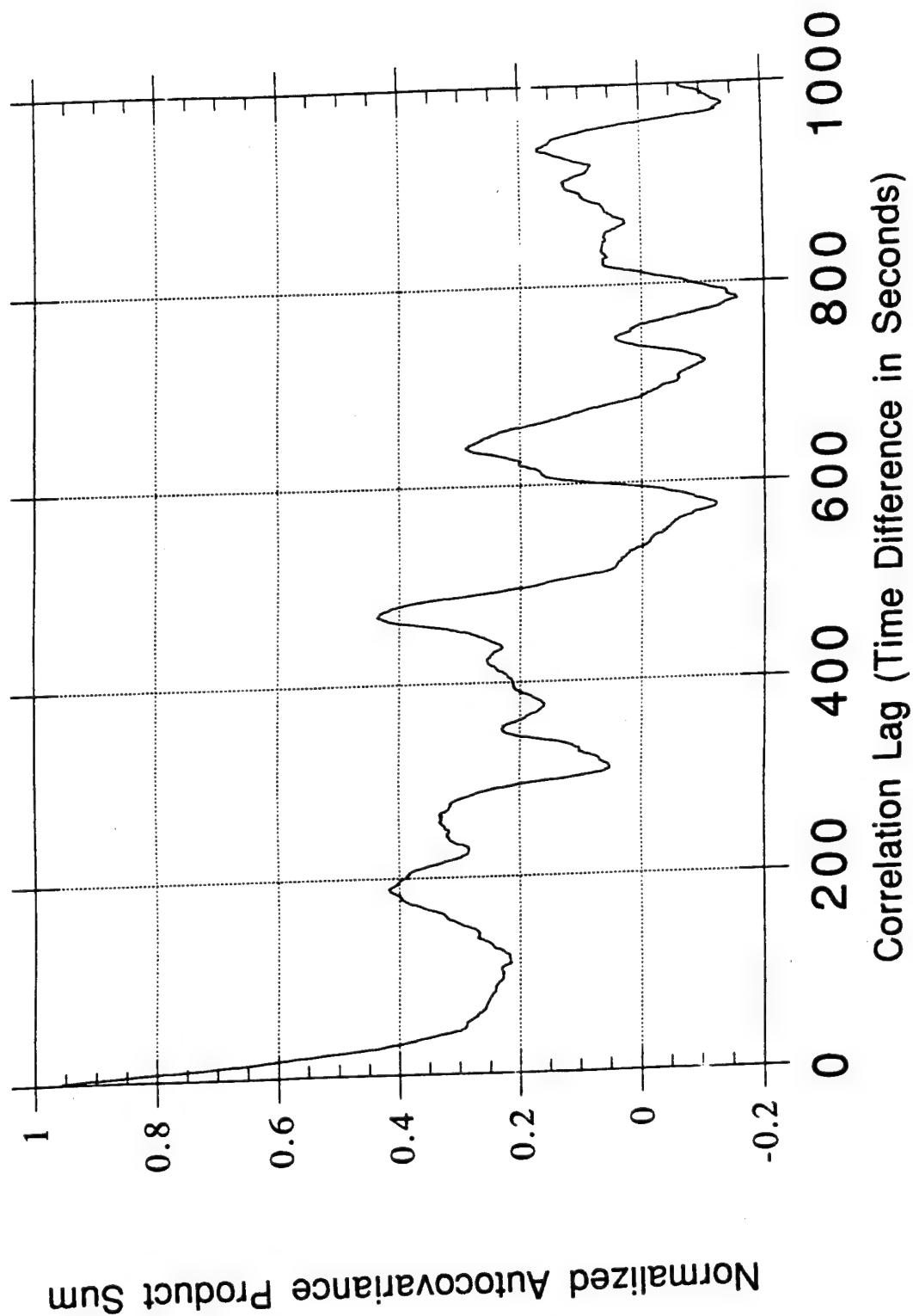
Figure 5-7. Autocorrelation function for wind speed during all flight between just 15.71666 and 16.12 hrs (UTC) or only passes 2-10 at FL 175.
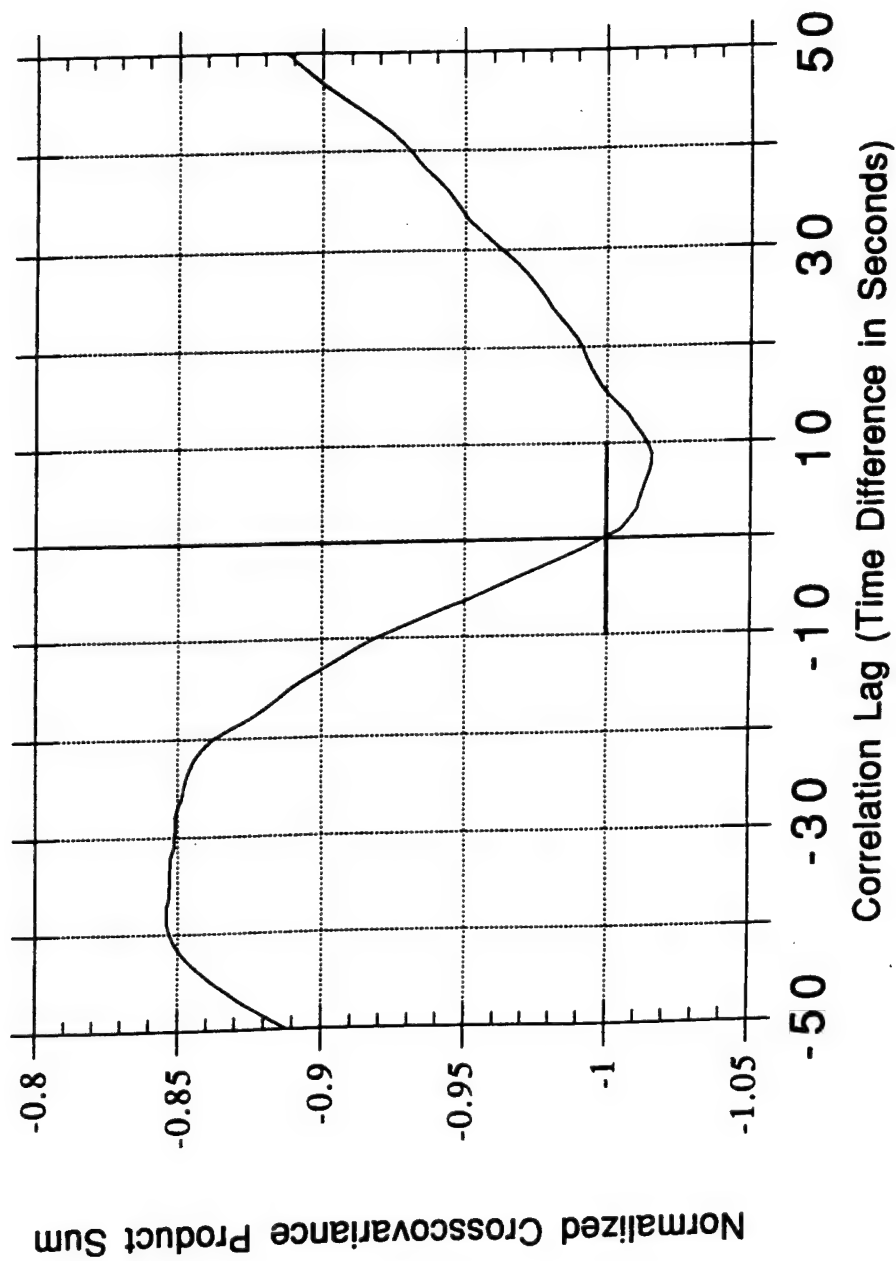
39

Figure 5-8. Cross correlation of vertical wind lagging ozone for 10 longer in-cloud times during sampling at FL 175.

5.7 PARTICLE SIZE DISTRIBUTIONS (PSDs) AND AREAL MASS CONCENTRATIONS.

Figure 5-9 shows some averaged PSDs from the four probes, including all of the bins in the three overlap intervals. The first/bottom one or two bins of each sensor should not be considered as accurate as the larger size bins due to the significant signal quantization and threshold effects. The good PSD aspect is that the valley feature at sub-micrometer sizes is seen by both pertinent probes. The bad aspect is that both FSSPs (the center two ranges) have intra-range PSD drops (at 8 and 57 μm, respectively) that are unusual and apparently unrelated. Both PSD drops are where an overlapping probe for larger sizes does not have enough resolution to lend any insight or confirmation; a few of the smallest 2D-C bins should be shifted right significantly for non-spherical shapes. There is no reason to exclude such sharp PSD drops, because some postulated special or strange net agglomeration effects can occur given the seven (7) molecules of water vapor for each one of CO_2 and one of N_2 in a perfect reaction of the ANFO ($3NH_4NO_3 + CH_2$).

The Figure 5-9 ordinate of cross-sectional particulate area is used intentionally so suspected effects of size bin cross-talk, etc. can be addressed, due to the sensors strictly responding to an optically effective particle area. There is an increased likelihood due to the peak power variations produced by the real scattering that the particles with the same physical size can be located in more than one or two bins for each probe. The jitter of the FSSP-300 data for ~1 μm diameter sizes indicates a possible systematic variation in the bin width from an ideal dust calibration curve with resonance effects. For example, doubling and halving the width for adjacent pairs of bins could lead to a smooth line for the six points from 0.8 to 2 μm diameter.

A virtual reference line of minus one slope on Figure 5-9 indicates that a mass concentration plot peaks around approximately 20 μm diameter. This is consistent with an associated vertical slip speed of only the order of ~2 cm/sec. Assuming that these sized particles are very efficiently locked into the cloud mixing flow suggests a mean mixing velocity of the order of ten times higher, which is ~20 cm/sec or 0.2 m/sec vertically. Such a transport dominating speed could have been expected even for the decaying 'turbulence' after the cloud's buoyant stabilization in the stable upper air.

Excluding the first pass at the slightly lower FL 172, the in-cloud sampling took from 50 to 135 sec, which is ~5 to 14 km in length. Figure 5-4 shows that passes 4, 5 and 9 encountered significant material on the north side. Evidently the lighting or contrast was poor on the north side because each pass was in a turn on that end, as if the crew could not easily tell that the cloud was present. Given the sun's elevation angle of 55-60° at these times, the north region was apparently shaded by the sheared higher portion of the cloud; the sun's azimuth was only 105-110° from true north. Because the NCAR pilots did not use a drifting aimpoint displayed from the inertial system, they had to get well away from cloud in order to judge where its centroid was for each pass.
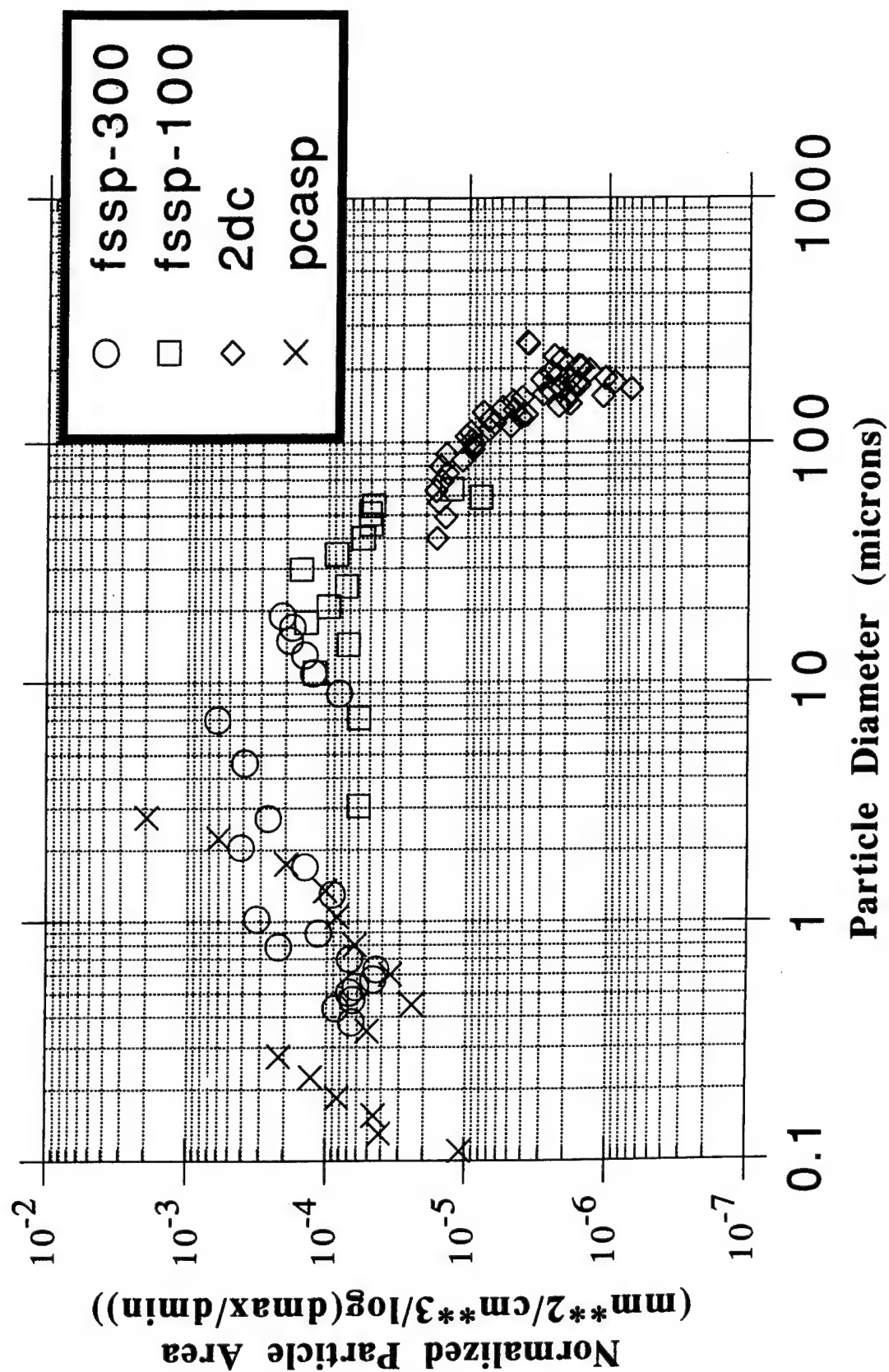
41

Figure 5-9. MINOR UNCLE distribution of normalized particulate cross-sectional area for FL 175 sampling.

The King Air also used a few filters for obtaining direct evidence of how much mass was ingested by the turboprop engines, an areal mass concentration. The ten passes at FL 175 from 1539 to 1607 UTC received 23 mg/cm². The 12 passes at FL 100 from 1631 to 1732 UTC received 12 mg/cm². A final 10 mg/cm², for a total of 45 mg/cm², was obtained on a following flight to search for any visible cloud fragments still present, whether detectable by the satellite or not. The latter areal mass concentration can also be used to verify the small probes' calibrations for dust due to the larger particles having fallen out by that time after burst and, thus, not being any interference.

5.8   SIZE CORRELATION MATRICES FOR PSD SENSORS.

The probable difference between the optically sensed sizes by flying the laser probes past the airborne particles and the small grains, etc. from the LANL filters after ashing the filters was addressed explicitly by using multiply designs of scattering probes for the MUDCAT. Many properties and features of the real particles and their optical characteristics produce variations in the observed peak power that is scattered out of the laser beam by individual particles. Thus, the different collector optics and pulse height analyzers in the scattering sensors can easily output apparently ambiguous data even for each probe; not an exclusive calibration of particle area to signal size. Dr. Baumgardner of NCAR/RAF is developing currently a higher technology airborne probe that is intended to reduce the size ambiguity for ice crystals and snowflakes. The nearly Gaussian-acting response or power scattering curve for a fixed particle surface area can smear the details of the actual PSD shape across more than just the adjacent areal sizes, which smooths out the actual PSD. The impact of the size ambiguity regarding each particle surface area increases as the peak powers are binned and the bin width is decreased for better PSD resolution. The following innovative investigation has been initiated in the attempt to quantify this so-called real world cross talk affect on the laboratory, etc. calibrations of the various scattering probes.

We have developed and applied a new technique to the large data base of observed event counts from an optical sizing by the peak scattered power for each detected particle. The technique is based on initially obtaining the regular Pearson correlation coefficient ('r') for every paired combination of particle size bins [i.e., n(n-1)/2] for a given run, covering a certain time interval, such as the n=15 bins of the PCASP. In the PCASP case, the off-diagonal triangular matrix has 105 Pearson correlation (r) values.

The trends among the matrix values of r will include the combined effects of the Poisson or counting jitter/uncertainty for the separate channel counts during equal time intervals, the strong self correlation (collinearity) among the channels that is inherent in the PSD, and the response tail for bins more remote than the two adjacent bins for larger and smaller sizes. The quantitative trends can be analyzed for both adjacent and remote bin dependence, or average statistical determination, by calculating the associated correlation or r^2 value for any matrix cell.

43

The (Pearson) correlation matrix is contaminated primarily by the collinearity among all of the size bins. This enhancement of each r^2 can mask the true r^2 relationship between bins when all the other variables/bins are held constant. The net result of the convey is easier to understand by forming the three-dimensional wire mesh surface plot of the correlation matrix. This display has revealed unexpected relationships or correlations that cause concern about the calibration, beam sampling area, and rejection performance of each sensor when the PSD has a unique shape. The real PSD shape is important in a dust cloud with condensed ANFO by-products, some of which may be on the dust particle surfaces and affecting the Mie scattering predictions and interpretations of the probe performance.

Figure 5-10 shows the summary of 688 counts for one second, with a non-zero count in the largest bin of the PCASP. This criterion was applied to suppress the count uncertainty effect enough that the whole wire surface is not biased downward. The counts came from the FL 175 sampling of the cloud and automatically exclude the turns due to the non-zero criterion. The grid starts in the lower left corner with bin 1 and goes to bin 15 on the right side; the number 4, 6, …, 12 denote the respective row and column intersections. While the ordinate minimum is an r of 0.6, the lowest plotted r value is around 0.68 for the point correlation between bins 4 and 15.

A major feature of the wire surface is that the first seven bins are highly correlated with each other, and the last eight bins (8-15) are nearly as highly self/cross correlated. More interesting is that the diagonal of the 14 correlations for only one bin away has a big dip for bins 7 and 8 and another dip for bins 11 and 12. One speculation is that this summary mixes parcels with two distinct narrow PSD modes, below bin 7 and between bins 8 and 11, that are separated spatially in the raw data. Given the previously noted inhomogeneities and asymmetries along some passes and the probable dry scavenging into larger powdery particles, such sub-micron and 'one' micron modes, respectively, are considered feasible.

Another major feature of the r surface is the plateau formed between bins 1 to 6 and bins 8 to 13, a 6 by 6 square with a systematically deeper dip for bin 9. The typical r^2 is only just above 50 percent so it is not necessarily a causal correlation. Such purely statistical correlations would be the case for an underlying smooth PSD with PSD humps that are due to spatially local processes, either now or earlier than the sampling time. Such postulated PSD spikes could simply fatten or broaden the whole systematically linear relationship between bins from an underlying smooth PSD and cause the observed systematic and significant step decease in r^2. Presumably the lower row 15 values for bins 1-6 are due to the onset of the effect from the uncertainty in low bin 15 counts. Accumulating all of the bin counts until there are over 10 particles in bin 15 would form fewer PSD samples for obtaining the correlation matrix but hopefully eliminate this cliff in the r surface.

Further insight into the sub- and supra-micron modes might be gained by inspecting an inter- or cross-probe correlation matrix. In this case, a large triangle matrix is formed from the two intra-probe triangles that are above and to the right of a rectangular matrix for the cross-probe matrix. Such a wire surface was formed for just the large particles seen by both the PCASP (the 7 bins
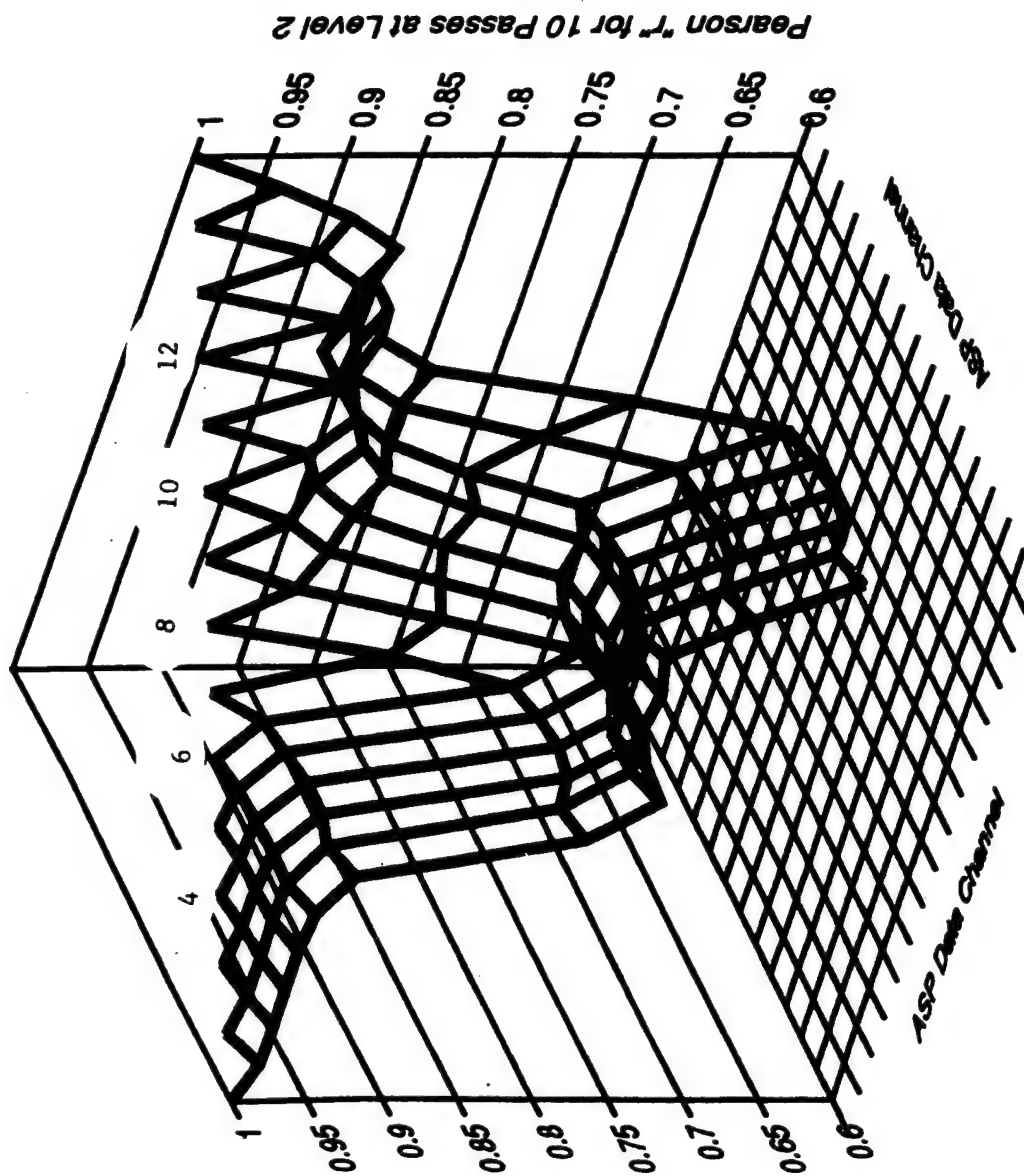
Figure 5-10. Wire surface formed by the correlation matrix (r values) for the PSDs observed by the PCASP (688 seconds when bin 15 is non-zero) during the 10 passes at FL 175.

45

9-15) and the FSSP-300 (the 13 bins 11-23) sensors. Ideally, the bin centers shown in Figure 5-9 indicate that a ridge should exist on the rectangle between the cell for plot variables 3 and 8 (i.e., PCASP bin 11 and FSSP-300 bin 11) and the cell for plot variables 7 and 12 (i.e., PCASP bin 15 and FSSP-300 bin 15). Two things are suggested by the absence of a ridge for these five points.

First, the low r values for the cross-probe correlations suggests that the PSD accumulation approach is needed to reduce the counting jitter on the implied scatter plots. Nevertheless, these low r values apparently uncovered a PCASP performance problem not noticed previously. PCASP bins 14 and 15 at minimum, plot variables 6 and 7, may be detecting just some portions of much larger particles. That is, plot variables 13 and 14 are the FSSP-300 bins 16 and 17 that are supposedly oversized for the PCASP. Thus, this timing simultaneity indicator variable r confirms the apparently biased data on figure 5-9 for PCASP bins 14 and 15, the highest two X symbols. Unfortunately, this discovered problem could have been masked by only using the suggested PSD accumulation approach.

The second suggestion is due to the essentially same r for the bins near the expected ridge and far from the expected ridge in the rectangle. That is, the collinearity effect is dominating the whole wire surface. Collinearity can be investigated systematically using the concept of partial correlation coefficients, which was applied recently by H. A. Singer at SAIC in the P-EARL program of code development (Versteegen et al., 1993).

The elements of the symmetric correlation matrix with values of r are the simple correlation coefficients expressing the correlation, that is, the strength of the linear association, between all possible pairs of variables. The square of the simple correlation coefficient r_{ij}, denoted by R^2_{ij}, is the coefficient of determination between the ith and j^{th} variables that quantifies the proportion of their variability explained by their mutual correlation. However, the variables x_i and x_j may be additionally correlated with any or all of the remaining N-2 variables. For this reason the r_{ij} are be called the simple (or zero-order, as explained below) correlation coefficients.

To isolate the correlation between each variable and just the ith variable requires the notion of partial correlation. Here, two variables are correlated while all other variables are held constant. For the case of only three variables, x_1, x_2 and x_3, the correlation coefficient between x_2 and x_3 for any fixed value of x_1 is called the partial correlation coefficient $r_{32.1}$. It is desired to express $r_{32.1}$ in terms of the simple correlations r_{32}, r_{21}, and r_{31}. It is shown in advanced texts (Kenney, 1949) that the first-order partial correlation formula is (any one variable held constant)

$$r_{32.1} = \frac{r_{32} - r_{31}\, r_{21}}{\sqrt{(1 - r_{31}^2)(1 - r_{21}^2)}}$$

The partial correlation coefficient value $r_{32.1}$ furnishes the true correlation between variables x_2 and x_3 in the sense that the interfering effects of variable x_1 are eliminated. The square of a partial correlation coefficient, the partial R^2, measures the relative amount of variability in the output variable attributable to a single input when all the remaining inputs are fixed. Hence after fixing x_1, $R^2_{32.1} = (r_{32.1})^2$ quantifies the proportion of the variability remaining in x_3 that is explained by its dependence upon x_2. The partial correlation matrix is also symmetric since $r_{23.1} = r_{32.1}$.

Let N denote the total number of variates. For $N \geq 3$ variates, the first-order partial correlation between the ith and j^{th} variables while holding a kth variable fixed is given by ($i < j \leq N$ and $k \neq i$ or j)

$$r_{ij.k} = \frac{r_{ij} - r_{ik} \, r_{jk}}{\sqrt{\left(1 - r_{ik}^2\right)\left(1 - r_{jk}^2\right)}}$$

where r_{ij}, r_{ik} and r_{jk} express the simple correlations between the respective i^{th}, j^{th} and k^{th} variables. There are $(N-2) \times C(N,2)$ distinct first-order partial correlations, where $C(N,2)$ denotes the number of different pairs (as combinations) that can be formed of the N variables, defined by

$$C(N, 2) = \frac{N!}{2! \, (N - 2)!}$$

and $N!$ is the factorial of N, i.e., $N! = N \times (N-1) \times (N-2) \times \ldots \times 2 \times 1$. Note that the order of the partial correlation refers to the number of variables being held fixed: no variables are fixed for a zero-order correlation, a single variable is fixed for first-order correlation, two variables are fixed for a second-order correlation, etc. up to a maximum of N-2 variables held fixed.

The formula for second-order partial correlations is a straightforward extension of the first-order formula above. For example, for $N \geq 4$ variates, the partial correlation between variables x_i and x_j while controlling for both x_k and x_l ($i, j, k, l \leq N$ and $i \neq j \neq k \neq l$) is given by the second-order partial correlation formula

$$r_{ij.kl} = \frac{r_{ij.k} - r_{il.k} \, r_{jl.k}}{\sqrt{\left(1 - r_{il.k}^2\right)\left(1 - r_{jl.k}^2\right)}}$$

where $r_{ij.k}$, $r_{il.k}$ and $r_{jl.k}$ are the first-order partial correlations among among the ith, j^{th} and k^{th} variables with the lth variable held fixed. Second-order partial correlation obey the symmetry relations $r_{ij.kl} = r_{ji.kl} = r_{ij.lk} = r_{ji.lk}$. There are $\frac{1}{2} [(N-3) \times (N-2)] \times C(N,2)$ distinct second-

order partial correlations, where $C(N,2)$ is defined as above. Higher-order partial correlation formulas can be set down recursively.

For the problem of modifying the two sensor calibration curves to solve which bins/channels are observing the same scatterers, it is hoped that only the fourth order partial correlations are needed. The larger and smaller bins around the presently perceived bin of both probes that match up would be held constant. If a sizing bias bigger than one bin is involved, then the firth or sixth order partial correlations could become involved. Presumably, one can just shift the bin pairing to capture any bias(es) by using other fourth order correlations than used originally, which were unsatisfactory.

By coincidence, the current bin 15 for both sensors is the same size of 2.75 μm diameter. In reality, some other FSSP-300 bin may be the better correlative for the PCASP bin 15. This is left as an exercise for some master's thesis dealing with the real world problems. It is unclear if enough dust particles were observed at each sampling altitude to permit partial correlation coefficients to be obtained with statistical significance. The plume sampling for the Kuwait Oil/gas Field Fire Experiment (KOFFE) may be the better statistical situation to use for the extensive calculations needed for obtaining partial correlation coefficients with many variables held fixed.

5.9 NOAA-9 IMAGES.

Numerous weather satellites are operated by the United States government. Due to an unforeseen shot timing change, hardly a better view could have been obtained. The forward scattered early morning sunlight went toward the NOAA-9 Polar Orbiting Environmental Satellite at an elevation angle of 63.5° on an azimuth from the Trinity site of 287°. Special processing of the ~10.8 and ~12 μm infrared band images was performed and presented in Cockayne and Edwards (1994).

5.10 WSMR PHOTOGRAPHS.

Numerous cameras were used at the event but none were planned more than the day before for the late time cloud. Fortunately, the documentary photography crew was able to prepare two large format still cameras with a one day notice. These were used upwind and crosswind to pan across the sheared dust cloud when the multi-wavelength satellite image was taken at 1557 UTC.

5.11 LANL FILTERS, PHOTOGRAPHS AND VIDEOTAPE.

Numerous changes were made in the LANL effort from its previous cloud sampling efforts. The first entry at low altitude at only 10 min after burst did show some multi-millimeter particles being present. They were not decelerated enough for the filter to prevent a simple penetration and loss. This caveat on larger sizes will be needed in order to compare particle size distributions from the filters with past early cloud measurements.

The mass concentrations were reported at the MINOR UNCLE D+60 Meeting on 21-22 September 1993, and in the MINOR UNCLE Dust Analysis Second Progress Report, October 4, 1993 (Mason and Finnegan, 1994). The LANL filters obtained the following;

Filter #	Alt^9(kft)	Time(min)	$Conc^{10}$(mg/m³)	Mass(g)	≤63μm(%)
2	7.7	10:19	80.4	2.3	30.0
3	9.4	12:25	205	6.0	29.0
4	11.1	14:25	198	9.2	49.1
5	12.4	16:35	179	7.3	13.7
6	14.1	19:08	58.9	3.4	35.1
7	15.7	24:47	55.4	4.2	14.7
8	17.3	27:08	18.9	1.5^{11}	41.1
9	14.6	32:00	37.0	6.2	16.1
10	10.7	36:17	31.1	1.4	61.3

The crew was innovative in operating a good videocamera in the cockpit. It gives a biased qualitative indication of the visibility conditions because the human eye sensitivity for other aircraft is much better, partially due to the perceived motion, and thus the visibility condition is not represented by a video (Personal communication, John Knollenberg, September 1993).Nevertheless, the video also provides the valuable complementary camera view of the early fireball rise and other motions. The other major contribution of the videotape is the distinct streaks recorded for the fragile particles hitting the side of the cockpit cover at small angles.

5.12 MUDCAT SUMMARY AND CONCLUSIONS.

Numerous measurements made by the sampling aircraft and other pertinent probes have built one of the most thorough dust cloud data bases ever collected. This data has been reduced from the SAIC perspective of what was learned and left unknown by previous sampling of large dust clouds. The poor records for whatever cause are identified and multiple opportunities for mixing and diffusion related investigations are suggested. Due to the calibration complexities, the desired dust cloud reconstruction from the upwind, crosswind and satellite images was not achieved herein.

---

[9] Mean radar reading for the pass entry and exit altitudes.

[10] Mean concentration subject to revision due to particle size effects on the sampled air volume.

[11] Mason and Finnegan (1994) reports that 7.6 % of the total mass was 125 mg of additional fibrous material, while all other passes had less than 1 % fibrous material.

The primary conclusion is that the sampling patterns of 10 to 12 passes were ideal for further data reductions and analysis to obtain real cloud growth behavior, whether or not driven by atmospheric turbulence. It is believed that these FL 175 and FL 100 sets are adequate for both mean translation code output comparisons as well as effective diffusion and dilution modeling comparisons. The 18 so-called passes for the FL 100 sampling came from fragmentation along some of the 12 azimuths flown based on the real time cloud view by the pilots from the cockpit.

The representative PSD for the FL 175 sampling around T + 45 minutes, shown in the Figure 7-1, can be approximated to first order using a single log-normal function that is a parabola on the log-log axes (Personal communication, Dr. Doug Youmans, 11 March 1994). The formula is the following for N = 2,300,000 particles per liter, or 2,300 particles per cm³;

$$dN/dln(d) = 2,300/[cm^3(2\pi)^{1/2}\ln(3.8)] \ \exp\{ - [\ln(d)-\ln(0.08 \ \mu m)]^2 \ / \ [2\ln^2(3.8)] \}$$

where the 3.8 is the geometric sigma, the one standard-deviation-factor multiplier and divider of the average diameter (0.08 μm) for the number concentration. Because Figure 5-9 is the cross-sectional area distribution, it is $\pi d^2/4$ times this equation. From the relatively small 0.08 μm mean of the particle count curve, the relatively large sigma significantly shifts the average diameter of particle area and its whole log-normal curve by a factor of $2\ln^2(3.8)$ along the natural logarithmic axis for particle size. Except for this shifting quantity, the ln everywhere can be replaced by log (i.e., log-base-ten). The shift from the 0.08 μm would then be $2\log(3.8)\ln(3.8)$, which in this case is 1.548 decades (i.e., factor of 35) to a 2.8 μm average of the particle area and thus 68% between 0.7 and 10.7 μm diameter. Such a broad particle size range suggests that the sunlight scattering is mainly forward for spherical particles, but the sphericity assumption is probably not valid.

5.13 MUDCAT RECOMMENDATIONS.

Numerous possible code comparisons can be proposed with this unique data base. The post stabilization by-products and dust diffusion in a free troposphere remains an oversimplified issue to which these detailed data should most certainly be addressed. The primary recommendation is to use more realistic techniques than the simple spectral flow characterizations that are applied standardly for fully developed turbulence/mixing. Even the so called intermittent turbulence technique is probably not applicable to this gas cloud and dust diffusion due to the significant stability in the free troposphere air. The rapidly decaying turbulent mixing as the cloud stabilized is potentially a unique event with extensive documentation and a thorough analysis is the minimum before force fitting this cloud's behavior into the existing categories used by the modelers. Another recommendation is that the modelers recognize the invalidation of the code calculations due to the lumping of the cloud by the cloud scale eddies in ambient air.

SECTION 6

CONCLUSIONS

The validation effort for the DNA/SPWE nuclear fireball/cloud calculations has made slow positive progress for assorted reasons. The primary problem appears to be the low program priority given to the detailed evaluations and resolution of the discovered discrepancies. For example, a factor of over 30 between the mass mean diameter for a stem sampling pass (7 min) at the MINOR SCALE shot and its post-shot 'prediction' was not addressed during this two year effort. This oversight occurred because the reviews of the predictions data base for the 91-series required reruns and post processor programming that consumed the 'validation' funding after the DICE code was modified significantly to use an adaptive algorithm for locally refining/coarsening the cell sizes every one to two/three time steps (the MAZ code). The net result was that the 91-series data base had to be subjected to major uncertainty excursions in its primary application as fratricide environments for strategic missiles. Unfortunately, a work around is not available at times much after stabilization due to the particulate settling domination of the physics by about 1,000 sec after burst.

In a separate evaluation report for this contract (Hillendahl, 1994), the MAZ output was processed to predict the bomb debris imagery as photographed after the IVY/King burst of an air-dropped weapon. The net result was that the temperatures in the MAZ output at around 2 sec after burst are excessively high. This was a surprise after the reasonably good DICE comparison (Hillendahl, 1993) and its cause could be either or both the radiation loss parameterization or the reduced diffusion in small cells injected automatically by MAZ.

This contract obtained the first full set of gas and particulate diffusion data from a dust cloud above the planetary boundary layer. The overview in section 5 is complemented by a more detailed version as a separate discussion and data presentation (Cockayne and Edwards, 1994). The net result is that an evaluation can now be performed for the details of every realization that is implied by the methodology in the Second Order Closure Turbulence Model (SOCTM), which is embedded in the DICE-MAZ code for treating the transport of the gases and dust particles/pebbles from the burst. The focus of the evaluation should be the representativeness of the local densities, where the scale of the local average is varied upward from the SOCTM-assumed Lagrangian length of 10 percent of the fireball/cloud size. Whether or not this Lagrangian length basis is validated is important because it determines implicitly the effective spatial resolution and gradient maximum for the dust densities in each particulate size bin used by DICE-MAZ and TASS.

In summary, this two years of effort raised many serious concerns about the fidelity to reality for the dust cloud calculations, even in any ensemble sense. Equally important, the value of sensitivity studies has been altered by the attractor attribute of the output from the adaptive zoned predictions.

51

SECTION 7

RECOMMENDATIONS

The primary recommendation is that the characteristics of the adaptive algorithm as implemented in the MAZ code be published for broad better understanding of its subtle effects. One issue is the periodic effect(s) of the domain coarsening by a factor of four for all of the finest spaced region(s) when the total cell count reaches some set limit, which completely purges all of the fine scale information. A complementary issue is the continuous/cumulative effect from an inherent numerical diffusion between coarse cells due to the short time steps dictated by some small cell divided by its high sound speed, which steadily purges all of the large and small scale information where the coarse cells are located. A third issue is the factors and their relative weightings, for airbursts and surface bursts, in the MAZ adaptivity algorithm rules for both refining and coarsening cells by a factor of four. These issues arise from fundamental concerns about the physical meaning of all the spatial details that differentiate the new predictions from previous predictions. Because the early excess fireball temperature again directly implies that reasonable results result from the wrong path at some points in the fireball/cloud evolution, any or all of the new details can be artificial despite any apparent agreement at the qualitative level. This caveat is germane due to the inability of doing numerically converged calculations with MAZ with the present DNA computational support.

The secondary recommendation is further exploration of the empirical dust data from events such as the well sampled MINOR UNCLE event using ANFO HE and the early sampled first three shots of Operation GREENHOUSE, which are 47-225 kT nuclear bursts on short towers so most of the airborne particles were not radioactive (Engquist and Goodale, 1951). This effort should focus on understanding the GREENHOUSE particulate microphysics and associated fractionation by using the Radioactivity Attachment Model (Simmons et al., 1993) to perform sensitivity studies using the output of the best available radiation and shock hydrocode for such tower bursts. Likewise, the MINOR UNCLE gas and particulate data should be interacted with the recently revised DICE-MAZ version with its particle-particle processes. These items arise from fundamental concerns about the persistent problem of PSD predictions not matching the in situ probe observations, even after accounting for the probe performance uncertainties.

52

SECTION 8

REFERENCES

Allen, J. T., 1993, "Reality Checkup; A Recovering Policy Junkie on True-Life Health Reform," The Washington Post, Sunday, October 10, 1993, pp C1-C2. Unclassified

Bacon, B. P. et al., 1992: "Single Burst Nuclear Cloud Database Volume 3--Model Validation and Special Studies," DNA-TR-92-11-V3, Science Applications International Corporation. Unclassified

Baumgardner, D., 1989: "Airborne Measurements for Cloud Microphysics," Research Aviation Facility Bulletin 24, National Center for Atmospheric Research. Unclassified

Blackman, R.B. and Tukey, J.W., 1959: The Measurement of Power Spectra, Dover, New York. Unclassified

Cockayne, J.E. et al., 1987: "Dust Cloud Diagnostics and Characterization for the MINOR SCALE Event," DNA-TR-87-210, Science Applications International Corporation. Unclassified.

Cockayne, J.E., and R.C. Edwards, 1992: "Dust Cloud Characterization for the MISTY PICTURE Event," DNA-TR-91-34, Science Applications International Corporation. Unclassified.

Cockayne, J. E., 1993: "Review of Selected Nuclear Cloud Experiments," DNA-TR-92-43, Science Applications International Corporation. Unclassified

Cockayne, J.E., and R.C. Edwards, 1994: "Dust Cloud Characterization for the MINOR UNCLE Event," Chapter 8 in the following reference; McCrory, R.,1994: MINOR UNCLE Symposium Report, POR 7453-3. Unclassified

Cooper, W.A., 1994: "Dispersion of Smoke Plumes From the Oil Fires of Kuwait." NCAR Technical Note NCAR/TN-402+STR. National Center for Atmospheric Research. Unclassified

Engquist, E.H., and T.C. Goodale, 1951: "Cloud Phenomena: Study of Particulate and Gaseous Matter." Unpublished

Flueck, J. A., 1989: "Some Past and Present Techniques in Evaluation of Model Fields," Proceedings of the 11th Conference on Probability and Statistics in Atmospheric Sciences, October 1-5, 1989, Monterey, CA.; Amer. Met. Soc. Unclassified

Halpert, M.S., G.D. Bell, V.E. Kousky, and C.F. Ropelewski, Editors, 1994: Fifth Annual Climate Assessment--1993, Climate Analysis Center. Unclassified

Hassig, P. A. et al., 1992: "Advances in Nuclear Cloud Modeling," DNA-TR-92-23, The Titan Corporation--California Research and Technology Division. Unclassified

Hillendahl, R. W., 1992: "The PROBE Code." Unpublished

Hillendahl, R. W., 1994: "PROBE Code Application to the KING Event," DNA-TR-93-154, Science Applications International Corporation. Unclassified

Kenney, J.F., 1949: Mathematics of Statistics: Part Two, Van Nostrand, New York. Unclassified

Meneveau, C., 1992: "Comment on 'Is intermittent motion of outer flow in the turbulent boundary layer deterministic chaos?' [Phys. Fluids A 3, 1941 (1991)]," Phys. Fluids A 4, 1587-1588. Unclassified

Murphy, A. H., 1991: "Forecast Verification; Its Complexity and Dimensionality," Mon. Wea. Rev., 119, 1590-1601. Unclassified

Norment, H.G., 1979: "DELFIC: Department of Defense Fallout Prediction System; Volume I--Fundamentals," DNA 5159F-1, Atmospheric Science Associates. Unclassified

Oreskes, N. et al., 1994: "Verification, Validation, and Confirmation of Numerical Models in the Earth Sciences," Science, 263, 641-646. Unclassified

Saaty, T.L., 1988: Mathematical Methods of Operations Research, Dover, New York. Unclassified

Shelton, F.H., 1988: "Reflections of A Nuclear Weaponeer," Shelton Enterprise, Inc., Colorado Springs, CO. Unclassified

Simmons, J.A. et al., 1993: Radioactivity Attachment Model, DNA-TR-93-92, Science Applications International Corporation. Unclassified

Stoddard, J. et al., 1994: RV Fratricide Methodologies: Upgrades and Applications of the Fratricide Prediction Model, DNA-TR-93-166, Science Applications International Corporation. Unclassified

Versteegen, P.L., et al., 1993: P-EARL An Aircraft Response Model (ARM), DNA-TR-92-183, Science Applications International Corporation. Unclassified

DISTRIBUTION LIST

DNA-TR-93-155

DEPARTMENT OF DEFENSE

DEFENSE INTELLIGENCE AGENCY
    ATTN: DIW-4

DEFENSE NUCLEAR AGENCY
    ATTN: OPNA
    ATTN: RAEM
    ATTN: RAST W SUMMA
    ATTN: SPWE LTC JIM HODGE
    ATTN: SPWE LTC MARK BYERS
    ATTN: SPWE LTC KENNE
2 CY ATTN: SSTL

DEFENSE TECHNICAL INFORMATION CENTER
2 CY ATTN: DTIC/OC

FIELD COMMAND DEFENSE NUCLEAR AGENCY
    ATTN: FCPR

DEPARTMENT OF THE ARMY

U S ARMY ATMOSPHERIC SCIENCES LAB
    ATTN: SLCAS-AR-M

U S ARMY NUCLEAR & CHEMICAL AGENCY
    ATTN: MONA-NU DR D BASH

U S ARMY TRAINING AND DOCTRINE COMD
    ATTN: ATCD-N

US ARMY CHEMICAL SCHOOL
    ATTN: ATZN-CM-CC-003

DEPARTMENT OF THE NAVY

NAVAL SURFACE WARFARE CENTER
    ATTN: CODE H-21

DEPARTMENT OF THE AIR FORCE

AIR UNIVERSITY LIBRARY
    ATTN: AUL-LSE

ASSISTANT CHIEF OF STAFF
    ATTN: AFSAA/SAK

DEPARTMENT OF ENERGY

LAWRENCE LIVERMORE NATIONAL LAB
    ATTN: TECH LIBRARY

LOS ALAMOS NATIONAL LABORATORY
    ATTN: TECH LIBRARY

SANDIA NATIONAL LABORATORIES
    ATTN: TECH LIB 3141

DEPARTMENT OF DEFENSE CONTRACTORS

JAYCOR
    ATTN: CYRUS P KNOWLES

KAMAN SCIENCES CORP
    ATTN: D MOFFETT
    ATTN: DASIAC

KAMAN SCIENCES CORPORATION
    ATTN: DASIAC

SCIENCE APPLICATIONS INTL CORP
2 CY ATTN: J E COCKAYNE
    ATTN: J MCGAHAN
2 CY ATTN: R C EDWARDS